Electron avoidance: A nonlocal radius for strong correlation

Lucas O. Wagner and Paola Gori-Giorgi

Department of Theoretical Chemistry and Amsterdam Center for Multiscale Modeling, FEW, Vrije Universiteit, De Boelelaan 1083,
1081HV Amsterdam, The Netherlands

We present here a model of the exchange-correlation hole for strongly correlated systems using a simple nonlocal generalization of the Wigner-Seitz radius. The model behaves similarly to the strictly correlated electron approach, which gives the infinitely correlated limit of density functional theory. Unlike the strictly correlated method, however, the energies and potentials of this model can be presently calculated for arbitrary geometries in three dimensions. We discuss how to evaluate the energies and potentials of the nonlocal model, and provide results for many systems where it is also possible to compare to the strictly correlated electron treatment.

I. INTRODUCTION

Treating strong electronic correlation at an affordable computational cost is an important missing building block for a truly predictive computational material science, chemistry, and biochemistry [1,2]. Though each strongly correlated system seems to require a new model and method, there are some powerful tools for probing these systems. Specialized wave-function methods such as the density-matrix renormalization group [3,4] yield impressive results for lattice models [5] and enjoy some success in describing real continuum systems [6–8], but they scale poorly with system size in three dimensions, and thus are limited as far as system size is concerned. On the other hand, Kohn-Sham density-functional theory (KS-DFT) [9], for which most approximations scale very well with system size, is often considered a method suited only for weakly correlated systems. The very first approximation in KS-DFT, the local-density approximation (LDA) [9], describes well the physics and energies of weakly correlated electrons, but can fail badly for strongly correlated systems, where the wave function is radically different than that of the KS noninteracting reference system. (In some communities, failure of KS-LDA is taken as the *definition* of strong correlation.) All standard KS-DFT approximations build upon LDA in one way or another [10–13], achieving greater accuracy in weakly correlated systems. In systems where KS-LDA is qualitatively wrong, however, fine-tuned improvements seem to have little hope of succeeding.

Despite this grim outlook, recent work has uncovered a functional which is correct in the strongly correlated limit—the strictly correlated electron (SCE) functional [14–16], defined as the minimum possible expectation value of the electron-electron repulsion in a given electron density. The SCE functional depends in a highly nonlocal way on the density [17,18]. This nonlocality is a new step in the strategy to construct more accurate approximate functionals by using information of increasing complexity (and computational effort)—sometimes called "Jacob's ladder" [19,20]. Traditionally, the steps of the ladder include local information (the value of the density at each point in space, yielding, e.g., LDA, LSDA [9,21]), semilocal information (density gradients, giving generalized gradient approximations (GGA's) [10,11,22]), the local KS kinetic-energy density (metaGGA's [23]), the occupied KS

orbitals (hybrids [12,24], self-interaction corrections [25,26], etc.), up to the KS virtuals (double hybrids [27], random-phase approximation in different flavors [28], etc.). As we will see, the nonlocal step utilizes information about certain *integrals* of the density; there are other such functionals (e.g., the weighted density approximation [29–33]), and we will introduce another in this work.

When applied in the self-consistent KS-DFT framework [17], the KS-SCE method correctly describes strong correlation phenomena such as bond dissociation [34] and charge localization in one-dimensional (1D) and two-dimensional (2D) traps with weak confinement [18,35], without introducing any artificial symmetry breaking. There are still challenges to meet before KS-SCE is ready for practical applications, however. In the three dimensional (3D) case, algorithms to compute the SCE functional are currently applicable only to spherically symmetric systems, although progress is being made by several groups exploiting the formal similarity between the SCE problem and optimal transport (or mass transportation) theory [36–41], a field of mathematics and economics [42]. Another crucial point is that SCE requires suitable corrections [34,43] (e.g., local or semilocal) to make it useful for chemistry and solid-state physics, where both the strong and the weak correlation regimes need to be treated accurately by the same methodology. Despite these challenges, hybridizing with the SCE functional (or an approximation thereof) holds the promise of remedying strong correlation failures in present KS-DFT functionals.

In this work, we present an approximation to the SCE functional, which is easier to implement for arbitrary geometries and may more readily accept corrections. The primary ingredient for this functional is a nonlocal generalization of the Wigner-Seitz radius. With this nonlocal Wigner-Seitz radius, we build a very natural (and nonlocal) model of the strong-interaction limit of the exchange-correlation hole. We call the resulting functional the nonlocal radius (NLR) functional. Previous attempts to build approximations for the SCE limit were based on local or semilocal information [44,45]. These models can be energetically accurate, but they miss nonlocality in the functional derivative—nonlocality which is necessary to self-consistently build features such as barriers that localize the charge density [17,18,35]. With the nonlocal Wigner-Seitz radius, our functional captures, self-consistently, some of the physics of strong correlation.

The paper is organized as follows. Since the exchange-correlation hole [46,47] and the strictly correlated electron approach are both useful in understanding our model, we discuss some relevant background on KS-DFT, SCE, and the exchange-correlation hole in Sec. II. We then present the nonlocal KS-NLR functional and its properties in Sec. III. The KS-NLR method is similar to some other nonlocal approximations, such as the weighted density approximation [29–33], and may be considered as a (nonlocal) simplification of the point-charge plus continuum (PC) model [44,48], so we discuss these relationships also in Sec. III. Finally, we compare self-consistent KS-SCE and KS-NLR calculations for a few systems in Sec. IV, where it becomes clear that these two methods behave quite similarly.

Though the nonlocal aspect of the KS-NLR functional offers its own set of integration challenges, evaluating the functional and its functional derivative with respect to the electron density is straightforward. To show this, we calculate the nonlocal functional for real 3D atoms—self-consistently for two electrons, and non-self-consistently for more—where the KS-SCE functional has also been evaluated [49]. We also treat the 3D hydrogen molecule non-self-consistently, which has only recently been treated by the exact KS-SCE functional [40,50]. In comparing the KS-NLR and KS-SCE methods, we also consider a simplified 1D universe, as in Ref. [51], where self-consistent calculations can be carried out very rapidly. There we discover that the nonlocal functional is capable of dissociating a single bond (such as in H_2 or LiH) correctly, as well as localizing charge density in 1D parabolic traps without symmetry breaking, just like the KS-SCE method [18]. We therefore consider the KS-NLR approach a presently viable alternative to KS-SCE that opens many doors in the development of strongly correlated KS-DFT methods.

II. BACKGROUND

Most investigations into electronic structure begin with the Born-Oppenheimer approximation. This allows the quantum electronic problem to be solved first, and then any quantum (or classical) nuclear effects to be added in later. The electronic Hamiltonian is

$$\hat{H} = \hat{T} + \hat{W} + \hat{V}, \tag{1}$$

with operators for the kinetic energy $\hat{T}$, electron-electron interaction $\hat{W}$, and potential energy $\hat{V}$. For a system of N electrons, these quantities may be written in the position representation as (using atomic units):

$$
\left.
\begin{aligned}
\hat{T} &\equiv -\sum_{i=1}^{N} \frac{1}{2} \nabla_i^2 \\
\hat{W} &\equiv \sum_{\substack{j>i}}^{N} \frac{1}{|\mathbf{r}_i - \mathbf{r}_j|} \\
\hat{V} &\equiv \sum_{i=1}^{N} v(\mathbf{r}_i)
\end{aligned}
\right\}, \tag{2}
$$

where $v(\mathbf{r})$ is the external potential usually coming from classical nuclei:

$$v(\mathbf{r}) = -\sum_{\alpha} \frac{Z_\alpha}{|\mathbf{r} - \mathbf{R}_\alpha|}, \tag{3}$$

where Z_α ($\mathbf{R}_\alpha$) is the charge (position) of the αth nucleus. Minimizing Eq. (1) over properly antisymmetrized wave functions yields the ground-state electron wave function Ψ, which is the key to many properties of the system.

Due to theorems by Hohenberg and Kohn [52], we can write the expectation values of all the operators in Eq. (2) as functionals of the electron density $n(\mathbf{r})$. For $\hat{T}$ and $\hat{W}$, this is accomplished by the constrained search formalism [53,54], where the internal energy of the system (kinetic plus electron-electron repulsion) is minimized over wave functions Ψ constrained to yield the density $n(\mathbf{r})$:

$$F[n] \equiv T[n] + W[n] \equiv \min_{\Psi \to n} \langle \Psi | \hat{T} + \hat{W} | \Psi \rangle, \tag{4}$$

where the minimizing Ψ is denoted $\Psi[n]$. For systems with degeneracy, a suitable generalization to mixed states $\Psi[n] \to \Gamma[n]$ is required, with a trace replacing the bra-ket in Eq. (4) [55–59]. The ground-state energy and density are then obtained through a minimization over reasonable densities [54] integrating to a certain desired particle number N:

$$E_v[n] \equiv T[n] + W[n] + \int d^3r \, n(\mathbf{r}) \, v(\mathbf{r}), \tag{5}$$

$$E_v(N) \equiv \min_{n \to N} E_v[n]. \tag{6}$$

Kohn-Sham DFT. The most widely applied DFT is Kohn-Sham DFT (KS-DFT) [9], which uses a set of fictitious noninteracting electrons to capture (in part) the Fermi statistics of the real system. In Kohn-Sham theory, the energy of Eq. (5) is partitioned as

$$E_v[n] \equiv T_{\mathrm{S}}[n] + \int d^3r \, n(\mathbf{r}) \, v(\mathbf{r}) + E_{\mathrm{HXC}}[n], \tag{7}$$

where $T_{\mathrm{S}}[n]$ is the kinetic energy of a set of noninteracting electrons with density $n(\mathbf{r})$, and $E_{\mathrm{HXC}}[n]$ is the Hartree-exchange-correlation energy which incorporates all effects due to electron interaction.

The functional derivative of Eq. (7) reveals a gradient-descent procedure for minimizing $E_v[n]$ [59], and leads to a set of equations which must be solved self consistently for the electron density $n(\mathbf{r})$:

$$v(\mathbf{r}) + v_{\mathrm{HXC}}[n](\mathbf{r}) = v_{\mathrm{S}}(\mathbf{r}), \tag{8}$$

$$\left\{ -\frac{1}{2} \nabla^2 + v_{\mathrm{S}}(\mathbf{r}) \right\} \phi_j(\mathbf{r}) = \epsilon_j \, \phi_j(\mathbf{r}), \tag{9}$$

$$2 \sum_{j=1}^{N/2} |\phi_j(\mathbf{r})|^2 = n(\mathbf{r}), \tag{10}$$

where $v_{\mathrm{HXC}}[n](\mathbf{r})$ is the Hartree-exchange-correlation (HXC) potential, the functional derivative of $E_{\mathrm{HXC}}[n]$:

$$v_{\mathrm{HXC}}[n](\mathbf{r}) \equiv \frac{\delta E_{\mathrm{HXC}}[n]}{\delta n(\mathbf{r})}, \tag{11}$$

and, for simplicity, we have considered a spin-unpolarized system (equal numbers of spin-up and spin-down electrons: $N_\uparrow = N_\downarrow = N/2$). In the KS scheme, one solves the above KS equations iteratively, until self-consistency is achieved [33]. The ground-state energy may then be computed by evaluating $E_{HXC}[n]$ with the converged density and the KS kinetic energy $T_S[n]$ using the converged KS orbitals:

$$T_S[n] = -\sum_{j=1}^{N/2} \int d^3r \, \phi_j^*(\mathbf{r}) \nabla^2 \phi_j(\mathbf{r}). \qquad (12)$$

For non-self-consistent densities, $T_S[n]$ must be evaluated using some other approach, e.g., via inversions [60–67].

So far we have only rewritten the original electronic structure problem; with the exact $E_{HXC}[n]$ functional, KS calculations are even more difficult than solving the electronic Hamiltonian in Eq. (1) directly [59]. The overwhelming practical success of KS-DFT is that $E_{HXC}[n]$ breaks up into pieces which can be more easily modeled. One can split $W[n]$ and $T[n]$ into pieces, which can be reassembled into $E_{HXC}[n]$:

$$\left.\begin{array}{l} W[n] \equiv W_H[n] + W_{XC}[n] \\ T[n] \equiv T_S[n] + T_C[n] \end{array}\right\}, \qquad (13)$$

where $W_H[n]$ is the Hartree energy of a density $n(\mathbf{r})$, often denoted by $E_H[n]$ or $U[n]$, $W_{XC}[n]$ is the interaction XC energy, composed of the exchange energy $E_X[n] = W_X[n]$ and the interaction correlation energy $W_C[n]$, and $T_C[n]$ is the kinetic correlation energy.[1] The full correlation energy $E_C[n]$ contains both kinetic and interaction contributions:

$$E_C[n] = W_C[n] + T_C[n], \qquad (14)$$

but no simple explicit expression exists for either (or both) of these terms. Finally, one obtains $E_{HXC}[n] = E_H[n] + E_{XC}[n]$, with $E_{XC}[n] = E_X[n] + E_C[n]$.

Energies from the XC hole. All of the interaction terms in Eq. (13) can be naturally written as Coulomb integrals. The true $W[n]$ can be found using the pair density $P(\mathbf{r},\mathbf{r}')$ of the interacting system:

$$P(\mathbf{r},\mathbf{r}') = N(N-1) \sum_{\sigma_1,\ldots,\sigma_N} \int d^3r_3 \ldots d^3r_N$$
$$\times |\Psi(\mathbf{r}\sigma_1,\mathbf{r}'\sigma_2,\mathbf{r}_3\sigma_3,\ldots,\mathbf{r}_N\sigma_N)|^2, \qquad (15)$$

with the full interaction energy being

$$W[n] = \frac{1}{2} \int d^3r \int d^3r' \, \frac{P(\mathbf{r},\mathbf{r}')}{|\mathbf{r}-\mathbf{r}'|}. \qquad (16)$$

Unfortunately, $P(\mathbf{r},\mathbf{r}')$ cannot be varied directly to determine $W[n]$ (though see Ref. [68] for an excellent discussion).

---

[1]Sometimes $W_C[n]$ of Eq. (13) is called the *potential* correlation energy, or written $U_C[n]$. However, the authors consider *interaction* correlation energy to more appropriately describe the correlation energy due to the Coulomb considerations. It must be clarified, however, that both $T_C[n]$ and $W_C[n]$ are a result of electron interaction: $T_C[n]$ is the increase in kinetic energy due to electrons avoiding each other more, while $W_C[n]$ is the decrease in Coulomb interaction energy.

Instead, the pair density must be modeled in some way, and in KS-DFT this is done through the density. The pair density is thus broken up into the following terms which are easier to model:

$$P(\mathbf{r},\mathbf{r}') = n(\mathbf{r})[n(\mathbf{r}') + h_{XC}(\mathbf{r},\mathbf{r}')], \qquad (17)$$

where $h_{XC}(\mathbf{r},\mathbf{r}')$ is the exchange-correlation hole, which has some simple properties summarized below.

Plugging $P(\mathbf{r},\mathbf{r}')$ (17) into $W[n]$ (16), we can obtain the various interaction energies of Eq. (13). The Hartree piece is

$$W_H[n] \equiv \frac{1}{2} \int d^3r \int d^3r' \, \frac{n(\mathbf{r}) \, n(\mathbf{r}')}{|\mathbf{r}-\mathbf{r}'|}, \qquad (18)$$

while the exchange-correlation piece is

$$W_{XC}[n] \equiv \frac{1}{2} \int d^3r \, n(\mathbf{r}) \int d^3r' \, \frac{h_{XC}(\mathbf{r},\mathbf{r}')}{|\mathbf{r}-\mathbf{r}'|}. \qquad (19)$$

Some approximations consider exchange and correlation separately, often when hybridizing with Hartree-Fock [12,13,24]. These approximations use the exact exchange hole in whole or in part:

$$h_X(\mathbf{r},\mathbf{r}') \equiv -\frac{1}{2} \frac{|\gamma_S(\mathbf{r},\mathbf{r}')|^2}{n(\mathbf{r})}, \qquad (20)$$

where $\gamma_S(\mathbf{r},\mathbf{r}')$ is the one-body reduced density matrix of the KS system:

$$\gamma_S(\mathbf{r},\mathbf{r}') = 2 \sum_{j=1}^{N/2} \phi_j(\mathbf{r}) \, \phi_j^*(\mathbf{r}'). \qquad (21)$$

While the foregoing allows one to evaluate the interaction XC energy $W_{XC}[n]$ for some given XC hole $h_{XC}(\mathbf{r},\mathbf{r}')$, the kinetic correlation energy $T_C[n]$ cannot directly be found through the XC hole. This is a consequence of using a noninteracting reference (i.e., the KS reference) and its kinetic energy $T_S[n]$. To get both $T_C[n]$ and $W_{XC}[n]$, one must integrate from the KS system to the fully interacting system using the adiabatic connection formalism [69,70]. This requires an infinite number of fictitious systems, all with density $n(\mathbf{r})$, but whose electron-electron repulsion is scaled by a factor of λ called the coupling constant. The ground-state wave functions $\Psi^\lambda[n]$ thus minimize the expectation value of $\hat{T} + \lambda\hat{W}$ under the constraint of giving the density $n(\mathbf{r})$, as in Eq. (4). Then $\Psi^0[n]$ is the KS wave function [likely a Slater determinant of the occupied KS orbitals $\phi_j(\mathbf{r})$], and $\Psi^1[n]$ is the true wave function of the system.[2] The full XC energy can then be found by an average of the XC holes from coupling constant $\lambda = 0$ to 1:

$$E_{XC}[n] = \frac{1}{2} \int d^3r \, n(\mathbf{r}) \int d^3r' \, \frac{\bar{h}_{XC}(\mathbf{r},\mathbf{r}')}{|\mathbf{r}-\mathbf{r}'|}, \qquad (22)$$

where the coupling-constant averaged XC hole is

$$\bar{h}_{XC}(\mathbf{r},\mathbf{r}') = \int_0^1 d\lambda \, h_{XC}^\lambda(\mathbf{r},\mathbf{r}'). \qquad (23)$$

---

[2]For systems with degeneracy, the coupling-constant wave functions Ψ^λ should be replaced by coupling-constant mixed states Γ^λ.

The XC hole at coupling constant λ, $h_{XC}^\lambda(\mathbf{r},\mathbf{r}')$, comes from the pair density $P^\lambda(\mathbf{r},\mathbf{r}')$ of the wave function $\Psi^\lambda[n]$, as in Eq. (17). Because $h_X^\lambda(\mathbf{r},\mathbf{r}')$ comes from the KS orbitals (which are the same for all λ), $\bar{h}_X(\mathbf{r},\mathbf{r}') = h_X(\mathbf{r},\mathbf{r}') = h_X^\lambda(\mathbf{r},\mathbf{r}')$.

Properties of the XC hole. The XC hole has some simple properties due to the properties of $P^\lambda(\mathbf{r},\mathbf{r}')$ [46]. The pair density is non-negative, so

$$h_{XC}^\lambda(\mathbf{r},\mathbf{r}') \geqslant -n(\mathbf{r}') \quad \forall \mathbf{r},\mathbf{r}'; \tag{24}$$

the pair density integrates over $\mathbf{r}'$ to yield $(N-1)\,n(\mathbf{r})$, which means that

$$\int d^3r'\, h_{XC}^\lambda(\mathbf{r},\mathbf{r}') = -1, \qquad \forall \mathbf{r}; \tag{25}$$

and utilizing the symmetry of the pair density (invariance under $\mathbf{r} \leftrightarrow \mathbf{r}'$), one can show:

$$\int d^3r'\, n(\mathbf{r}')\, h_{XC}^\lambda(\mathbf{r}',\mathbf{r}) = -n(\mathbf{r}), \qquad \forall \mathbf{r}. \tag{26}$$

These properties are ideal to build into models for $h_{XC}(\mathbf{r},\mathbf{r}')$, but many approximate functionals have XC holes which do not satisfy them. For example, the local-density approximation (LDA) [9] corresponds to the XC hole of the uniform electron gas [71]. The LDA XC hole is properly normalized (25), but does not always satisfy Eq. (24) [e.g., in certain circumstances when $n(\mathbf{r}) > n(\mathbf{r}')$]. The spherical average $\bar{h}_{XC}(\mathbf{r}; u)$ of the XC hole is defined as

$$\bar{h}_{XC}(\mathbf{r}; u) \equiv \frac{1}{4\pi} \int_{4\pi} d\Omega_{\hat{u}}\, \bar{h}_{XC}(\mathbf{r}, \mathbf{r} + u\hat{u}). \tag{27}$$

The LDA usually provides a good approximation of the short-range part (small u) of the system average of Eq. (27), i.e., $n(\mathbf{r})\,\bar{h}_{XC}(\mathbf{r}; u)$ integrated over all space [72–74]. If an XC hole is considered as a model of this spherical average, then Eq. (26) cannot be directly assessed [47]; whether one thinks of LDA as an approximation to $h_{XC}(\mathbf{r},\mathbf{r}')$ or $h_{XC}(\mathbf{r}; u)$, therefore, informs on whether LDA should satisfy Eq. (26) or not. Regardless, the correct normalization of the LDA XC hole [as in Eq. (25)] is a significant factor in the robustness of LDA [75]. The forerunner to PBE [10,76] forced normalization of the XC hole to cure problems with the gradient expansion of the density [73], giving insight into the need for the generalized gradient approximation (GGA).

Strictly correlated electrons. The strictly correlated electron (SCE) functional [14–18] corresponds to the $\lambda \to \infty$ limit of the adiabatic connection formalism, completely opposite to the Kohn-Sham system at $\lambda = 0$. The basic building blocks of the SCE method are called *co-motion* functions, and are analogous to KS orbitals in KS-DFT. Instead of minimizing the kinetic energy, however, the co-motion functions minimize the interaction energy for a given density [14,15,17,18]. The co-motion functions $\mathbf{f}_j(\mathbf{r})$ with $j = 1, \ldots, N$ thus pinpoint classical locations of the electrons. Setting $\mathbf{f}_1(\mathbf{r}) = \mathbf{r}$ to be the position of one electron, we can write the interaction energy of the SCE method as [15,77,78]

$$W_{SCE}[n] \equiv \frac{1}{2} \int d^3r \sum_{i=2}^{N} \frac{n(\mathbf{r})}{|\mathbf{r} - \mathbf{f}_i(\mathbf{r})|}, \tag{28}$$

where the co-motion functions minimize this expression and satisfy the two following physical constraints.

Because of the indistinguishability of electrons, the co-motion functions must satisfy cyclic group properties. Therefore knowledge of any nontrivial co-motion function $\mathbf{f}_i(\mathbf{r})$ is enough to generate all others:

$$\left.\begin{aligned}
\mathbf{f}_1(\mathbf{r}) &\equiv \mathbf{r} \\
\mathbf{f}_2(\mathbf{r}) &\equiv \mathbf{f}(\mathbf{r}) \\
\mathbf{f}_3(\mathbf{r}) &= \mathbf{f}(\mathbf{f}(\mathbf{r})) \\
&\vdots \\
\mathbf{f}_{N+1}(\mathbf{r}) &= \underbrace{\mathbf{f}(\mathbf{f}(\ldots \mathbf{f}(\mathbf{f}(\mathbf{r}))))}_{N \text{ times}} = \mathbf{r}
\end{aligned}\right\}. \tag{29}$$

Here we used $\mathbf{f}_2(\mathbf{r})$ as the *comotion generator* $\mathbf{f}(\mathbf{r})$ to produce the entire set.

In the SCE method, measuring the position of one electron also determines all others; therefore the probability of finding an electron at position $\mathbf{r}$ must be the same as finding an electron at any $\mathbf{f}_i(\mathbf{r})$ for $i = 2, \ldots, N$. Thus the comotion generator $\mathbf{f}(\mathbf{r})$ must satisfy the nonlocal differential equation [15]:

$$n(\mathbf{r}) = |J(\mathbf{r})|\, n(\mathbf{f}(\mathbf{r})), \tag{30}$$

where $J_{\mu\nu}(\mathbf{r}) = \partial f_\mu(\mathbf{r})/\partial r_\nu$ are the Jacobian matrix elements of $\mathbf{f}(\mathbf{r})$, and $|J(\mathbf{r})|$ is the determinant. Alternatively, Eq. (30) can be expressed as an integral equation:

$$\int_\Omega d^3r\, n(\mathbf{r}) = \int_{\mathbf{f}(\Omega)} d^3r\, n(\mathbf{r}), \tag{31}$$

where Ω is an arbitrary volume, and $\mathbf{f}$ maps Ω to the volume $\mathbf{f}(\Omega)$, i.e., $\mathbf{f}(\Omega) \equiv \{\mathbf{f}(\mathbf{r}) \,\forall\, \mathbf{r} \in \Omega\}$.

In one dimension, we can find the co-motion functions as explicit functionals of the density, without performing the minimization implicit in Eq. (28) [17,79]. For spherically symmetric 2D and 3D problems, the radial components of the co-motion functions can also be found quite easily, while the angular components require minimizing the interaction energy over the electronic angles [15,35,78]. But for a general 3D geometry, determining the co-motion functions is not as simple. There is no shortcut; the co-motion functions come out of $W_{SCE}[n]$ being minimized subject to constraints (29) and (30). There is an alternative approach to evaluate $W_{SCE}[n]$, the Kantorovich dual formulation [36,39], which bypasses the co-motion functions, and proves feasible for nonspherical systems.

It seems promising to develop approximations for the co-motion functions, since they have a physically transparent meaning and role. However, we proceed along somewhat different lines to develop our functional for strongly correlated systems.

III. A NONLOCAL MODEL OF THE XC HOLE FOR STRONG CORRELATION

In this section we present our model for the XC hole in the strong-interaction limit, the nonlocal radius (NLR) XC hole, and describe the properties of the resulting NLR energy functional and its functional derivative. We present some non-self-consistent results with the NLR functional on exact atomic densities, both real atoms and 1D pseudoatoms, and compare to the SCE functional. The NLR model can be thought of as

a real-space version of self-interaction correction [25,26], and it may be a descendant of the weighted density approximation [29–33] on one side and the PC model [44,48] on the other; we discuss this likely ancestry after introducing the concepts of the nonlocal NLR functional. For further comparisons, we evaluate the NLR functional and others on the uniform electron gas.

The key ingredient for our NLR XC functional is a nonlocal generalization of the Wigner-Seitz radius, inspired by work on orbital-free kinetic-energy functionals [80]. We define this nonlocal Wigner-Seitz radius $R(\mathbf{r})$ implicitly as the radius of the sphere centered at $\mathbf{r}$ which encloses one electron:

$$\int d^3 r' \, n(\mathbf{r}') \, \theta(R(\mathbf{r}) - |\mathbf{r}' - \mathbf{r}|) \equiv 1, \quad (32)$$

where $\theta(x)$ is the Heaviside step function, equal to 0 for $x < 0$ and 1 otherwise. This is a simple generalization of the usual Wigner-Seitz radius r_S, which can be similarly defined in the uniform gas, using $\mathbf{u} = \mathbf{r}' - \mathbf{r}$, $u = |\mathbf{u}|$:

$$\int d^3 u \, n \, \theta(r_S - u) \equiv 1, \quad (33)$$

and which for nonuniform systems is typically generalized in a local way: $r_S(\mathbf{r}) \equiv (3/(4\pi n(\mathbf{r})))^{1/3}$. The Wigner-Seitz radius has been used to characterize the uniform electron gas from the beginning [81], since it quantifies an effective distance between electrons. The nonlocal generalization $R(\mathbf{r})$ reduces to the local radius $r_S(\mathbf{r})$ for uniform systems, but it offers greater physical insight about the average number of electrons near each point in a nonuniform system.

We now use the nonlocal information contained within the nonlocal Wigner-Seitz radius $R(\mathbf{r})$ to design a model XC hole which is correct for one-electron-like systems, e.g., in dissociating H_2, as well as one-electron systems. Our XC hole sets the pair density to zero for electron coordinates within the nonlocal radius:

$$h_{XC}^{NLR}(\mathbf{r},\mathbf{r}') = -n(\mathbf{r}') \, \theta(R(\mathbf{r}) - |\mathbf{r}' - \mathbf{r}|). \quad (34)$$

This NLR XC hole models systems in which the electron wave function allows no two electrons to get close to each other, i.e., systems which are strongly correlated. This means that $h_{XC}^{NLR}(\mathbf{r},\mathbf{r}')$ is an approximation for the $\lambda \to \infty$ limit of the XC hole—the SCE hole—and not the coupling constant averaged hole $\bar{h}_{XC}(\mathbf{r},\mathbf{r}')$. In much the same way, SCE physics describes the situation in which each electron excludes the others from a volume in which the density integrates to 1. Therefore, if we approximate $\bar{h}_{XC}(\mathbf{r},\mathbf{r}')$ by $h_{XC}^{NLR}(\mathbf{r},\mathbf{r}')$, we expect to obtain energies far too low for most chemical systems, just like in KS-SCE [17,34].

For efficiency of notation, it is convenient to define the volume $\Omega(\mathbf{r})$ over which the Heaviside step function of (32) is nonzero. The volume $\Omega(\mathbf{r})$ is defined as the sphere centered at $\mathbf{r}$ with radius $R(\mathbf{r})$, so that we can rewrite Eq. (32) as

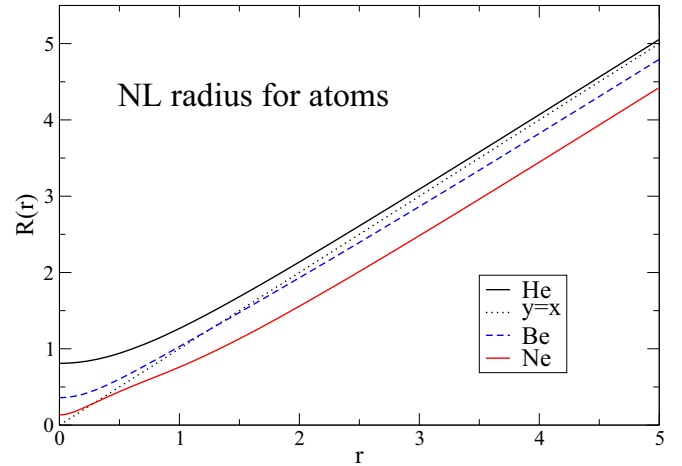$$\int_{\Omega(\mathbf{r})} d^3 r' \, n(\mathbf{r}') \equiv 1. \quad (35)$$

FIG. 1. (Color online) Nonlocal radius $R(r)$ (32) for the exact densities of the spherically symmetric atoms helium, beryllium, and neon; exact data from Refs. [82–84]. To see the asymptotic behavior, the $y = x$ line is also plotted.

Now plugging Eq. (34) into Eq. (19), we find the NLR interaction XC energy to be

$$W_{XC}^{NLR}[n] \equiv -\frac{1}{2} \int d^3 r \int_{\Omega(\mathbf{r})} d^3 r' \, \frac{n(\mathbf{r}) \, n(\mathbf{r}')}{|\mathbf{r} - \mathbf{r}'|}, \quad (36)$$

where the $\mathbf{r}'$ integral only integrates over the nonlocal volume $\Omega(\mathbf{r})$. Thus the hole of Eq. (34) completely removes the Hartree interaction between the density at $n(\mathbf{r})$ and $n(\mathbf{r}')$ if $\mathbf{r}'$ is within the sphere $\Omega(\mathbf{r})$ centered at $\mathbf{r}$.

To give an idea of what is going on inside the NLR XC model, we discuss some properties of the nonlocal (NL) radius $R(\mathbf{r})$. For $N \leqslant 1$ systems, $R(\mathbf{r}) \to \infty$, so that the NLR interaction XC energy cancels the Hartree energy, i.e., $W_{XC}^{NLR}[n] = -W_H[n]$. For all other (finite) systems, the NL radius asymptotically goes like $R(\mathbf{r}) \to r - c(\hat{r})$ as $r \to \infty$, where $c(\hat{r})$ depends on how many electrons there are, as well as the direction of $\mathbf{r}$ for nonspherical systems. We can easily calculate $R(\mathbf{r})$ for any given density by fitting the density to a sum of exponentials or Gaussians, and this is explained in Appendix A. In Fig. 1, we show $R(\mathbf{r})$ for a few atoms. The NL radius has bumps and curves due to shell structure, but these are rather gentle since $R(\mathbf{r})$ is defined by an integral over the density. Asymptotically, $c(\hat{r}) = 0$ for helium, and more generally $c(\hat{r}) = 0$ for any spherically symmetric $N = 2$ system. The next leading term in $R(\mathbf{r})$, a $1/r$ term with some small coefficient, explains why $R(\mathbf{r})$ for helium does not look yet like r for the larger r values in Fig. 1. In Fig. 2 we show a contour plot of $R(\mathbf{r})$ for the hydrogen molecule at bond length $R = 6$. Due to a lack of shell structure in H_2, $R(\mathbf{r})$ is rather bland and featureless. Its contours in the (z, ρ) plane are roughly ellipses which tend towards circles at large distances.

Functional derivatives. We can put $W_{XC}^{NLR}[n]$ into a symmetric form:

$$W_{XC}^{NLR}[n] = \frac{1}{2} \int d^3 r \int d^3 r' \, \frac{n(\mathbf{r}) \, n(\mathbf{r}')}{|\mathbf{r} - \mathbf{r}'|} \, g_{XC}^{NLR}(\mathbf{r},\mathbf{r}'), \quad (37)$$

where the NLR pair XC function is

$$g_{XC}^{NLR}(\mathbf{r}_1,\mathbf{r}_2) \equiv -\frac{1}{2}[\theta(R(\mathbf{r}_1) - r_{12}) + \theta(R(\mathbf{r}_2) - r_{12})], \quad (38)$$

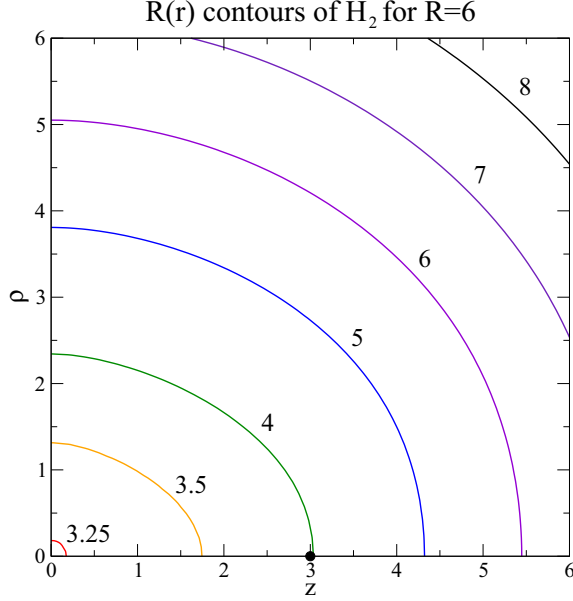## R(r) contours of H₂ for R=6

FIG. 2. (Color online) Nonlocal radius $R(\mathbf{r})$ (32) for the exact density of the H_2 molecule with bond length $R = 6$, in cylindrical coordinates (z, ρ). Exact density is the Full-CI result from GAMESS-US [85] within the aug-cc-pV6Z [86] basis set. The bond axis is along the z coordinate, and the nuclei are at $z = \pm 3$.

with $r_{12} \equiv |\mathbf{r}_1 - \mathbf{r}_2|$. The functional derivative can then be written with this pair XC function as

$$v_{\text{XC}}^{\text{NLR}}[n](\mathbf{r}) = \int d^3r' \, \frac{n(\mathbf{r}')}{|\mathbf{r} - \mathbf{r}'|} \, g_{\text{XC}}^{\text{NLR}}(\mathbf{r}, \mathbf{r}')$$
$$+ \frac{1}{2} \int d^3r' \, \frac{n(\mathbf{r}')}{R(\mathbf{r}')} \, \theta(R(\mathbf{r}') - |\mathbf{r} - \mathbf{r}'|), \quad (39)$$

and see Appendix B for a full derivation. The second term integrates over all points $\mathbf{r}'$ which are within their own Wigner-Seitz radius $R(\mathbf{r}')$ of the point $\mathbf{r}$. We call this region the NL reflection volume $\widetilde{\Omega}(\mathbf{r})$, and its definition is similar to the NL volume $\Omega(\mathbf{r})$:

$$\left.\begin{array}{l} \Omega(\mathbf{r}) \equiv \{\mathbf{r}' : R(\mathbf{r}) > |\mathbf{r} - \mathbf{r}'|\} \\ \widetilde{\Omega}(\mathbf{r}) \equiv \{\mathbf{r}' : R(\mathbf{r}') > |\mathbf{r} - \mathbf{r}'|\} \end{array}\right\}. \quad (40)$$

There is another such $\widetilde{\Omega}(\mathbf{r})$ integration region in the first term of Eq. (39) due to the NLR pair XC function. These integrals are straightforward, albeit numerically challenging, to evaluate.

By construction, the NLR XC hole satisfies the correct XC hole normalization in Eq. (25), in a nonlocal and physically meaningful way. In addition, the nonlocal XC hole satisfies another constraint on the exchange-correlation hole: Eq. (24), since $h_{\text{XC}}^{\text{NLR}}(\mathbf{r}, \mathbf{r}') \geqslant -n(\mathbf{r}')$. But since $h_{\text{XC}}^{\text{NLR}}(\mathbf{r}, \mathbf{r}')$ does not satisfy Eq. (26), $v_{\text{XC}}^{\text{NLR}}[n](\mathbf{r})$ does not go like $-1/r$ as $r \to \infty$ as it should. Instead, $v_{\text{XC}}^{\text{NLR}}[n](\mathbf{r}) \to -1/(2r)$ as $r \to \infty$. One can see this by examining Eq. (38) and Eq. (39). As $r \to \infty$, one step function inside $g_{\text{XC}}^{\text{NLR}}(\mathbf{r}, \mathbf{r}')$ will vanish—the term with $R(\mathbf{r}')$—since $R(\mathbf{r}')$ is rather small near the molecular center. Integrating the density at $n(\mathbf{r}')$ with the other step function yields exactly one electron, but with minus one-half out front

TABLE I. Evaluating the NLR functional on various exact 3D atomic densities, and comparing against exact numbers [82,83,87,88], the generalized gradient approximation (GGA) of the PC model [15], as well as the SCE model [15,49]. Exact densities from Refs. [15,82–84] are fitted to a sum of exponentials to evaluate $R(\mathbf{r})$ and thus $W_{\text{XC}}^{\text{NLR}}[n]$ as described in Appendix A. Lithium $E_{\text{XC}}[n]$ is done in a pure DFT way—i.e., with a set of spin-restricted KS orbitals—using the KS potential of Ref. [15] and the CCSD(T) = FULL results of the CCCBDB [89] using the aug-cc-pVQZ basis set [86].

Atom	$E_{\text{XC}}[n]$	$W_{\text{XC}}^{\text{NLR}}[n]$	$W_{\text{XC}}^{\text{PC-GGA}}[n]$	$W_{\text{XC}}^{\text{SCE}}[n]$
H⁻	−0.423	−0.543	−0.559	−0.569
He	−1.067	−1.426	−1.468	−1.498
Li	−1.799	−2.496	−2.556	−2.596
Be	−2.770	−3.835	−3.961	−4.021
Ne	−14.49	−18.28	−20.00	−19.99

[in Eq. (38)] and the Coulomb operator inside the integral in Eq. (39), the result is $v_{\text{XC}}^{\text{NLR}}[n](\mathbf{r}) \to -1/(2r)$.

Non-self-consistent results for atoms and molecules. In Table I, we evaluate $W_{\text{XC}}^{\text{NLR}}[n]$ for the exact densities of simple atoms and compare to SCE results and the exact $E_{\text{XC}}[n]$. As expected, for chemical systems $W_{\text{XC}}^{\text{NLR}}[n]$ is too low to approximate $E_{\text{XC}}[n]$. A generalized-gradient approximation to the PC model, PC-GGA [44], is also tabulated for these atoms. We discuss the PC model later in terms of NLR quantities, but here we note that its GGA incarnation $W_{\text{XC}}^{\text{PC-GGA}}[n]$ behaves energetically quite similarly to $W_{\text{XC}}^{\text{NLR}}[n]$, as does $W_{\text{XC}}^{\text{SCE}}[n]$. These strongly correlated methods are all lower than the exact $E_{\text{XC}}[n]$, but the nonlocal methods (KS-NLR and KS-SCE) are exact for one-electron systems. However, for H, PC-GGA does very well: the exact $E_{\text{XC}}[n] = -0.312500 = W_{\text{XC}}^{\text{NLR}}[n] = W_{\text{XC}}^{\text{SCE}}[n]$, while $W_{\text{XC}}^{\text{PC-GGA}}[n] = -0.312767$, an error of less than 0.1%. Notice however, that while energies can be very similar when the functionals are evaluated on accurate densities, the functional derivatives (potentials) behave very differently. For example, charge localization without magnetic order is obtained self-consistently by KS-SCE [18,35] and by KS-NLR (see Sec. IV), while it is missed by any local or semilocal functional.

As in other work [49], we compare interaction XC energy densities to understand the properties of the nonlocal functional. We define the interaction XC energy per particle $w_{\text{XC}}[n](\mathbf{r})$ as

$$w_{\text{XC}}[n](\mathbf{r}) \equiv \frac{1}{2} \int d^3r' \, \frac{h_{\text{XC}}(\mathbf{r}, \mathbf{r}')}{|\mathbf{r} - \mathbf{r}'|}, \quad (41)$$

so that $W_{\text{XC}}[n] = \int d^3r \, n(\mathbf{r}) \, w_{\text{XC}}[n](\mathbf{r})$. Like all energy densities, $w_{\text{XC}}[n](\mathbf{r})$ has a gauge, since the introduction of the Laplacian of any function, i.e., $w_{\text{XC}}[n](\mathbf{r}) \to w_{\text{XC}}[n](\mathbf{r}) + (\nabla^2 f[n](\mathbf{r}))/n(\mathbf{r})$, will give the same integral $W_{\text{XC}}[n]$ [90]. However, in Eq. (41), we have chosen the XC hole gauge where $w_{\text{XC}}[n](\mathbf{r}) \to w_{\text{X}}[n](\mathbf{r}) \to -1/(2r)$ as $r \to \infty$. In this gauge, the exchange energy per particle is [using Eq. (20)]

$$w_{\text{X}}[n](\mathbf{r}) = -\sum_{i,j=1}^{N} \frac{\phi_i^*(\mathbf{r}) \, \phi_j(\mathbf{r})}{n(\mathbf{r})} \int d^3r' \, \frac{\phi_j^*(\mathbf{r}') \, \phi_i(\mathbf{r}')}{|\mathbf{r} - \mathbf{r}'|}, \quad (42)$$
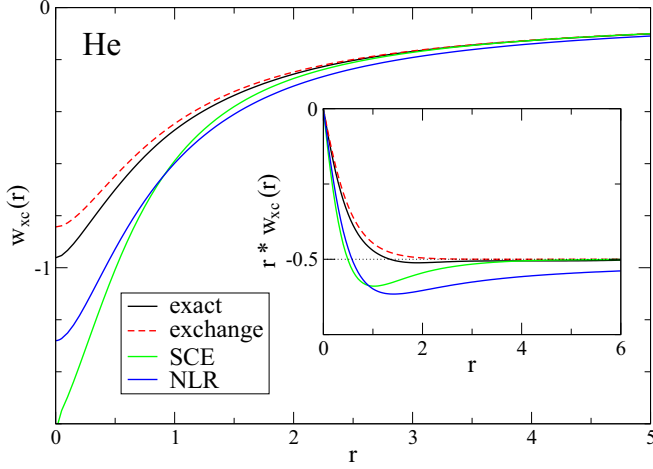
FIG. 3. (Color online) The interaction XC energy per particle (41) as a function of the radius r for the exact 3D helium atom density [49]. Inset: $r\,w_{XC}(\mathbf{r})$ to see asymptotic behavior. The exact $w_{XC}(\mathbf{r}) \to -1/(2r)$ as $r \to \infty$.

the SCE interaction energy per particle becomes [49]

$$w_{XC}^{SCE}[n](\mathbf{r}) \equiv \frac{1}{2}\sum_{i=2}^{N}\frac{1}{|\mathbf{r}-\mathbf{f}_i(\mathbf{r})|} - \frac{1}{2}v_H[n](\mathbf{r}), \qquad (43)$$

and the NLR interaction energy per particle is

$$w_{XC}^{NLR}[n](\mathbf{r}) = -\frac{1}{2}\int_{\Omega(\mathbf{r})}d^3r'\,\frac{n(\mathbf{r}')}{|\mathbf{r}-\mathbf{r}'|}. \qquad (44)$$

We plot these energy densities for various atoms: helium in Fig. 3, the hydrogen anion in Fig. 4, and beryllium in Fig. 5. For these systems, the exact $w_{XC}(\mathbf{r})$ lies below the exchange-only $w_X(\mathbf{r})$, above $w_{XC}^{NLR}(\mathbf{r})$, and usually above $w_{XC}^{SCE}(\mathbf{r})$. For beryllium at large r, however, the reverse
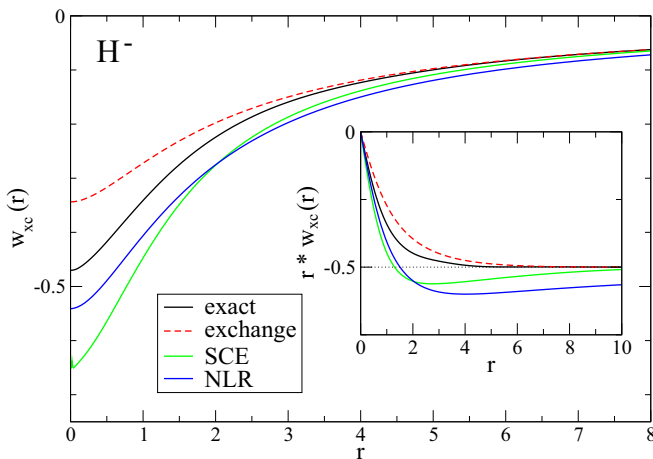

FIG. 4. (Color online) The interaction XC energy per particle (41) as a function of the radius r for the exact 3D H$^-$ atom density [49]. Inset: $r\,w_{XC}(\mathbf{r})$.
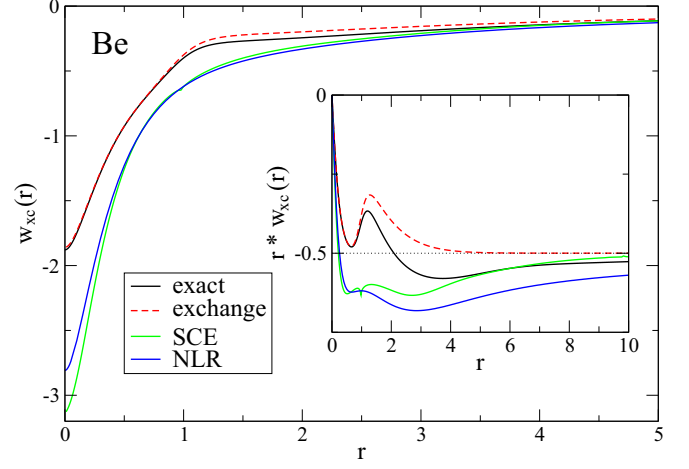

FIG. 5. (Color online) The interaction XC energy per particle (41) as a function of the radius r for the exact 3D beryllium atom density [49]. Inset: $r\,w_{XC}(\mathbf{r})$. Notice that the SCE energy density physically has a kink near $r = 1$, which has to do with classical electrons disappearing to infinity in the SCE method [49].

occurs.[3] One flaw of the NLR method is that its interaction XC energy per particle decays quite slowly to the correct $-1/(2r)$ behavior.

With the above properties, $w_{XC}^{NLR}(\mathbf{r})$ may be well suited as an ingredient to approximate the true $w_{XC}(\mathbf{r})$ using a local-weighting approach [49,91],

$$w_{XC}^{hyb}(\mathbf{r}) \equiv \frac{\alpha(\mathbf{r})\,w_{XC}^{NLR}(\mathbf{r}) + w_X(\mathbf{r})}{\alpha(\mathbf{r}) + 1}, \qquad (45)$$

where $\alpha(\mathbf{r})$ becomes large in regions where strong correlation effects are important, and goes to zero where HF is sufficient. While we will not pursue this idea any further in this work, we remark here that this may be seen as integrating $h_{XC}^{\lambda}(\mathbf{r},\mathbf{r}')$ to remove λ dependence in the adiabatic connection formalism using some local (or nonlocal) information at position $\mathbf{r}$ [49,91]. This local weighting is inspired by the interaction strength interpolation (ISI) method, which obtains $E_{XC}[n]$ directly by integrating a model of $W_{XC}^{\lambda}[n]$ [14,44,45,92]. The advantage of local weighting is that it is inherently size consistent, whereas the ISI is not [49].

We are also able to calculate H$_2$ within the KS-NLR method, which we present here non-self-consistently. This calculation is much more difficult for KS-SCE, due to the lack of a general 3D geometry solver. With KS-NLR, H$_2$ is rather straightforward, though the challenge is finding $R(\mathbf{r})$. As already seen in Fig. 2, $R(\mathbf{r})$ is a rather simple function, so we use a very simple grid exploiting the cylindrical symmetry of H$_2$. The result is in Fig. 6. We expected KS-NLR to be a lower bound to the energy, and it is clear from the figure that KS-NLR does poorly except for large bond distances (at very

---

[3]That $w_{XC}^{SCE}(\mathbf{r})$ can sometimes be above the exact $w_{XC}(\mathbf{r})$ is, while unusual, not too surprising. This has also been observed for the Hookium atom [49]. The basis set dependence is strong out in the tail region of these atoms, but to the scale of the figures we believe we are converged to the basis set limit.
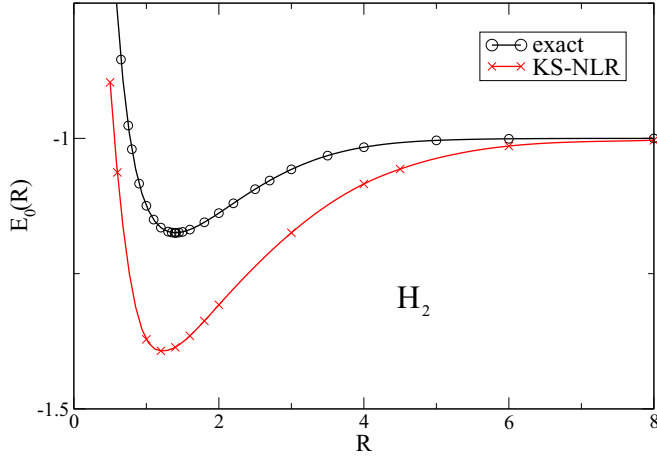
FIG. 6. (Color online) 3D H_2 comparing exact energies from Ref. [93] with non-self-consistent KS-NLR energies on exact densities; densities from GAMESS-US [85] Full-CI calculations within the aug-cc-pV6Z [86] basis set, with fits thanks to S. Vuckovic. Lines are cubic spline interpolations through data (at markers).

strong correlation). Nevertheless, the figure confirms what we would expect from KS-SCE considering 1D results [34] (and see later in this paper).

Ancestry and relatives. In his original approximation, Hartree corrects for self-interaction within the orbitals [94]:

$$W_{\mathrm{XC}}^{\mathrm{Hartree}} \equiv -\frac{1}{2} \sum_{\sigma} \sum_{i=1}^{N_\sigma} \int d^3 r \int d^3 r' \frac{|\phi_{i\sigma}(\mathbf{r})|^2 |\phi_{i\sigma}(\mathbf{r'})|^2}{|\mathbf{r}-\mathbf{r'}|},$$

(46)

where we include spin indices σ for the orbitals. For $N = 2$ electrons, this approximation is equivalent to Hartree-Fock, and with spin-symmetry breaking it is unrestricted Hartree-Fock. For $N > 2$ electrons, this approximation does not include exchange effects, however, and it is not invariant under unitary orbital rotations. In contrast, the NLR interaction XC energy $W_{\mathrm{XC}}^{\mathrm{NLR}}[n]$ *is* invariant under unitary transformations of the orbitals, since it only depends on the density (and the NL radius which can be found from the density). The NLR method can thus be thought of as a real-space version of self-interaction correction. One may compare more recent orbital-based corrections that are either nonunitary [25] or unitary [26], but look less like the NLR interaction XC energy than Eq. (46).

Due to including some nonlocal information about the density, the NLR functional is also similar in spirit to the weighted density approximation (WDA) [29–33], which uses the pair XC function of the uniform electron gas, but with an averaged version of the density to enforce the correct hole normalization. The functional is designed to be correct in the uniform gas, but to have an improved hole for nonuniform systems. Recent WDA's yield results of similar quality to GGA functionals (at a higher computational cost), but with the advantage of avoiding symmetry breaking (see, e.g., Ref. [95]).

Finally, the NLR functional appears to be most closely related to the point-charge plus continuum (PC) model [44,48]. The PC model finds inspiration from Wigner's treatment [96]

TABLE II. Evaluation of NLR (36), PC [with the NLR $\Omega(\mathbf{r})$] (47), and SCE interaction XC functionals on the exact density of 1D systems given soft-Coulomb interactions between electrons. Exact data and densities from Ref. [51]. Equilibrium (eq.) and stretched (str.) 1D H_2 are with bond lengths $R = 1.6$ and 5, respectively [51].

System	$E_{\mathrm{XC}}[n]$	$W_{\mathrm{XC}}^{\mathrm{NLR}}[n]$	$W_{\mathrm{XC}}^{\mathrm{PC}}[n]$	$W_{\mathrm{XC}}^{\mathrm{SCE}}[n]$
1D H$^-$	−0.595	−0.747	−0.727	−0.756
1D He	−0.733	−0.877	−0.871	−0.889
1D Li	−1.087	−1.288	−1.275	−1.303
1D Be	−1.481	−1.782	−1.788	−1.818
1D eq. H$_2$	−0.683	−0.836	−0.838	−0.846
1D str. H$_2$	−0.661	−0.700	−0.717	−0.713

of the strongly correlated, very-low-density ($r_S \gtrsim 100$) uniform electron gas, for which he was able to obtain accurate correlation energies. In the PC model [48], the XC energy is obtained as the electrostatic energy of an electronic system in a fictitious positive background with the same density $n(\mathbf{r})$. Specifically, one determines the electrostatic energy of a given cell $\Omega(\mathbf{r})$, wherein the density integrates to 1. [Previous work on the PC model uses local or semilocal approximations to $\Omega(\mathbf{r})$ [44], but for a closer comparison we use the nonlocal $\Omega(\mathbf{r})$.] The cell is modeled as one point-charge electron (at $\mathbf{r}$) and the positive background in the volume $\Omega(\mathbf{r})$. The cell energy is then the sum of the interaction of the point charge at $\mathbf{r}$ with the positive background and the background-background interaction in the cell. One then sums over and averages the energy of the cells [44,49]:

$$W_{\mathrm{XC}}^{\mathrm{PC}}[n] = -\int d^3 r\, n(\mathbf{r}) \int_{\Omega(\mathbf{r})} d^3 r' \frac{n(\mathbf{r'})}{|\mathbf{r}-\mathbf{r'}|}$$
$$+ \frac{1}{2} \int d^3 r\, n(\mathbf{r}) \int_{\Omega(\mathbf{r})} d^3 r' \int_{\Omega(\mathbf{r})} d^3 r'' \frac{n(\mathbf{r'})\, n(\mathbf{r''})}{|\mathbf{r'}-\mathbf{r''}|}.$$

(47)

Comparing Eq. (47) and Eq. (36), one might roughly think of $W_{\mathrm{XC}}^{\mathrm{NLR}}[n]$ as some approximation to $W_{\mathrm{XC}}^{\mathrm{PC}}[n]$—if each integral (without its coefficient) has about the same magnitude.

In Table II, we verify for some simple 1D pseudoatoms and molecules that using the nonlocal radius to define $\Omega(\mathbf{r})$ for the PC model results in energies very close to the nonlocal model, though neither is consistently closer to the exact $E_{\mathrm{XC}}[n]$. In one dimension we use soft-Coulomb interactions between electrons and nuclei: $w(u) = 1/\sqrt{u^2+1}$, with appropriate coefficients due to nuclear charges. Reference [51] explains the methodology for both exact and approximate solutions to these 1D systems; such model systems are analogous to simple 3D systems and allow quick evaluation and prototyping of functionals. The 1D H_2 data in Table II suggest that the PC model as well as the SCE model energies for the 3D H_2 molecule would be a little deeper and asymptotically slower to converge to the isolated atom limit than KS-NLR in Fig. 6. This may not be true for other molecules, however, which we will see later when considering 1D LiH. Despite the small advantage to KS-NLR for H_2, we reiterate that all of these nonlocal functionals give a very low estimate for $E_{\mathrm{XC}}[n]$.

We mention here that due to the triple integral in Eq. (47), the PC model would be *much* more expensive to implement self-consistently than the NLR functional. Unlike in the NLR model, the functional derivative of $W_{XC}^{PC}[n]$ does not simplify nicely, and one is left with single, double, and triple integrals just to evaluate the potential at one point, $v_{XC}^{PC}[n](\mathbf{r})$. This is true even if a local approximation to $R(\mathbf{r})$ is used, unless a local approximation is also applied to the integrals. Doing this, however, would destroy some of the nice properties of the PC model.

As a final remark on the PC model, we notice that if one uses the nonlocal $R(\mathbf{r})$ [and $\Omega(\mathbf{r})$] in the PC model, the corresponding XC potential has the right asymptotic behavior. In fact, the second term (the background self-interaction term) in Eq. (47) is short-ranged, and the first term is twice $W_{XC}^{NLR}[n]$. Since the long-ranged part of $v_{XC}^{NLR}[n](\mathbf{r})$ goes like $-1/(2r)$, the long-ranged part of $v_{XC}^{PC}[n](\mathbf{r})$ is thus twice that, or $-1/r$. This behavior is interesting and warrants further research.

The uniform electron gas. There is one many-body system where we can analytically investigate the behavior of these strong correlation functionals: the uniform electron gas, studied from days of yore [81,96].

In the uniform gas, $R(\mathbf{r}) \to r_S$, so we can easily calculate the per-particle energy of $W_{XC}^{NLR}[n]$ as a function of r_S:

$$
\begin{aligned}
w_{XC}^{NL-unif}(r_S) &= -\frac{1}{2} \int d^3 u\, n\, \theta(r_S - u)/u \\
&= -2\pi n \int_0^{r_s} du\, u \\
&= -\pi n r_S^2 = -0.75/r_S.
\end{aligned}
\tag{48}
$$

The local approximation to the NLR XC energy would thus be

$$
W_{XC}^{NL-unif}[n] \equiv \int d^3 r\, n(\mathbf{r})\, w_{XC}^{NL-unif}(r_S(\mathbf{r})).
\tag{49}
$$

The SCE functional gives the correct interaction XC energy for the strongly correlated (or low density) uniform electron gas [49]. The interaction XC energy per particle in this $r_S \to \infty$ limit is [44,81]

$$
w_{XC}^{SCE-unif}(r_S) \approx -0.895\,93/r_S.
\tag{50}
$$

The PC interaction XC energy per particle has also been calculated for the uniform gas [44],

$$
w_{XC}^{PC-unif}(r_S) = -0.9/r_S,
\tag{51}
$$

which is quite close to the exact low-density limit (see Ref. [49] for further discussion). We emphasize here that both $W_{XC}^{NLR}[n]$ and $W_{XC}^{PC}[n]$ are approximations to the strongly correlated limit, so they both make an error on the low-density uniform gas. However, the Wigner crystal is achieved only in the ultralow-density regime, around $r_S \gtrsim 100$. For perspective, r_S is about 100 at a distance of 7 Bohr radii from a hydrogen atom, so these limits may not be too useful in practice.

There is one observation that we should make given the above. Even though KS-NLR will give low energies for many systems of chemical interest, it will not necessarily yield a lower bound to the energy of any system (contrary to KS-SCE, which is guaranteed to yield a rigorous lower bound to the exact energy); in the ultralow density uniform electron gas we evidently have $E_v^{KS-NLR}[n] > E_v[n]$.

As we proceed, we leave behind the local $W_{XC}^{NL-unif}[n]$ (49). Using a local approximation in our interaction XC energy obviously nullifies the interesting nonlocal physics of the NLR functional, including its ability to capture one-electron and one-electron-like systems correctly. However, the uniform gas may have a different role to play when building corrections to KS-NLR, which we will address in future work.

IV. SELF-CONSISTENT NONLOCAL RESULTS

In this section, we use $W_{XC}^{NLR}[n]$ to approximate $E_{XC}[n]$ in the KS framework, and run self-consistent calculations for a few systems where it is also possible to compare to KS-SCE and exact results. We find that in many systems the KS-NLR functional behaves like the KS-SCE functional, differing only somewhat for anions.

The energy in the KS-NLR method is

$$
\begin{aligned}
E_v^{KS-NLR}[n] \equiv T_S[n] &+ \int d^3 r\, n(\mathbf{r})\, v(\mathbf{r}) \\
&+ W_H[n] + W_{XC}^{NLR}[n].
\end{aligned}
\tag{52}
$$

To perform self-consistent calculations with this functional, we must include $v_{XC}^{NLR}[n](\mathbf{r})$ in the KS potential:

$$
v_S^{NLR}(\mathbf{r}) = v(\mathbf{r}) + v_H[n](\mathbf{r}) + v_{XC}^{NLR}[n](\mathbf{r}).
\tag{53}
$$

Asymptotically, since $v_{XC}^{NLR}[n](\mathbf{r}) \to -1/(2r)$ as $r \to \infty$, we have

$$
v_S^{NLR}(\mathbf{r}) \to \frac{N - Z - \frac{1}{2}}{r} \qquad (r \to \infty),
\tag{54}
$$

where Z is the total charge of all nuclei in the system. The correct asymptote of $v_S(\mathbf{r})$, however, is $(N - Z - 1)/r$, which is very important in anions. Many standard LDA and GGA functionals have short-ranged $v_{XC}(\mathbf{r})$, however, so their asymptotic behavior is worse than the NLR functional. The exception is the B88 functional [11], which like the KS-NLR functional has half the right asymptotic behavior: $v_{XC}(\mathbf{r}) \to -1/(2r)$. For B88, this is enforced using the exponential decay of the density, however, which is true only for atoms and molecules. Within parabolic traps, therefore, the B88 functional needs modifications [97], while the NLR functional does not. The KS-SCE method is also density-decay indifferent, but its XC potential goes correctly to $-1/r$ as $r \to \infty$.

For our 3D results, we perform self-consistent atomic calculations by diagonalization on a simple radial grid (spherically averaging the density). We numerically integrate for the nonlocal radius $R(r)$ as well as the NLR XC potential $v_{XC}^{NLR}(r)$ each iteration. This simple NLRATOMS code is freely available online.[4] In one dimension, we use the machinery of Refs. [18,51] to self-consistently determine the energies of pseudoatoms and molecules.

A. 3D atoms

In this section we study real 3D atoms. We start with $N = 2$ (helium and hydrogen anion atoms), since KS-NLR gives the

---

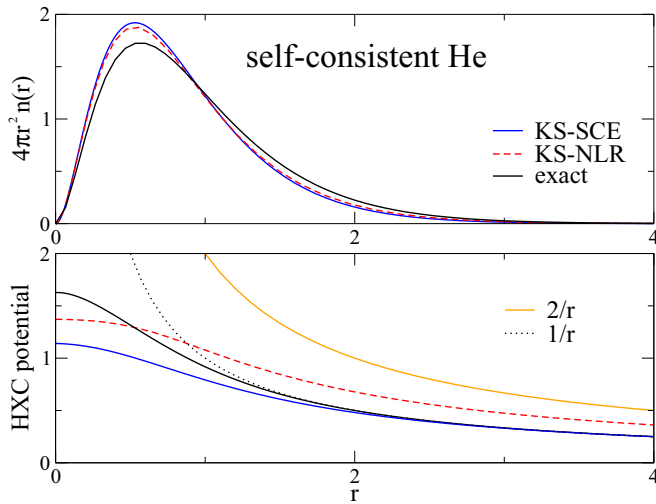[4]The basic KS-NLR code for atoms can be found at https://github.com/lowagner/NLRatoms.

FIG. 7. (Color online) Self-consistent results for the KS-SCE and KS-NLR (52) energy functionals of the 3D helium atom: plotted are the densities and HXC potentials, with comparisons to $1/r$ ($2/r$), the asymptotic behavior of the exact (LDA) HXC potential. Exact results thanks to C. Umrigar [82].

correct energies for $N = 1$ systems. We study the challenge of binding the hydrogen anion in KS-DFT by two methods: variable N from 0 to 2 with $Z = 1$, and fractional Z with fixed $N = 2$. Finally we consider ionization energies and the HOMO eigenvalues of the KS-NLR method for small atoms up to neon.

Helium. See Fig. 7 for a self-consistent treatment of the helium atom, both with the KS-NLR functional (52) and the KS-SCE functional. Both strong-correlation functionals gives a self-consistent energy which is low compared to the exact (-3.278 in KS-NLR and -3.357 in KS-SCE [43], whereas the true energy of helium is -2.904 [82]), and both also give a helium density much too contracted. This contraction gives KS-SCE and KS-NLR a larger kinetic energy and a more-negative potential energy than the exact helium atom. Comparing the strong correlation methods: the KS-SCE and KS-NLR self-consistent densities are very similar; the KS-NLR density decays a little more slowly due to a higher highest occupied molecular orbital (HOMO) eigenvalue, which can be seen in Fig. 9.

Hydrogen anion. While the NLR functional appears to be a lower bound for these finite systems, this does not mean that the NLR functional always binds when the true system does. We work through this paradox by considering the anion H^-. For the exact density $n(\mathbf{r})$ of the system, the NLR energy is less than the true energy, $E_v^{\mathrm{KS-NLR}}[n] < E_v[n]$, since $W_{\mathrm{XC}}^{\mathrm{NLR}}[n] < E_{\mathrm{XC}}[n]$ in Table I. Nevertheless, it appears that one can find a lower NLR energy $E_v^{\mathrm{KS-NLR}}[\tilde{n}]$ for some density $\tilde{n}(\mathbf{r})$ which sends a fraction of an electron to infinity. With a large enough basis set, this can be deduced from a positive HOMO eigenvalue in the self-consistent treatment, which we found when trying to converge H^- for KS-NLR.

Many standard DFT approximations behave exactly the same way for anions: in an infinite basis set, functionals such as B3LYP and PBE would send a fractional number of electrons to infinity [98]. Nevertheless, in Ref. [98],
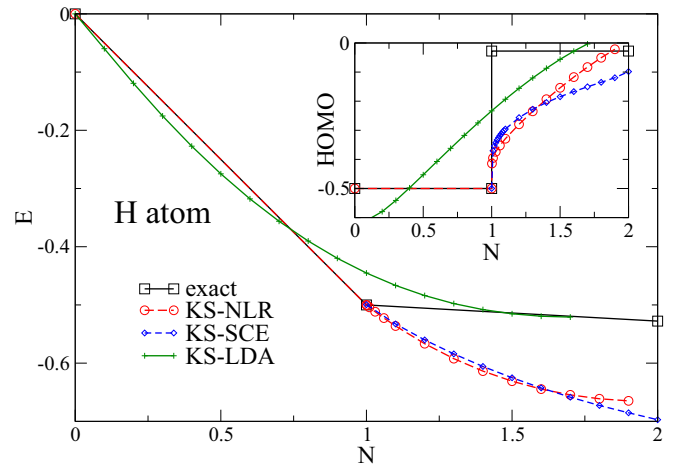

FIG. 8. (Color online) Self-consistent energies of the KS-NLR, KS-SCE, and KS-LDA methods for the hydrogen atom with a variable number of electrons N, performed within a spin-restricted framework. KS-SCE and KS-LDA data from Ref. [43].

Burke and co-workers find that these functionals can yield good electron affinities, if the anion is calculated with the functionals evaluated on densities with less error (in the atomic case Hartree-Fock densities). The functional evaluated on a good anion density has a lower energy than the functional self-consistently evaluated on the neutral system, giving a reasonable electron affinity for standard functionals [98]. As we have already seen, this is similar to the KS-NLR functional: the non-self-consistent energy of H^- is lower than the self-consistent KS-NLR energy of H, even though KS-NLR will not self-consistently bind an extra electron. With this approach, however, the KS-NLR electron affinity is a severe overestimation of the true electron affinity [$A^{\mathrm{KS-NLR}} = 0.148$ whereas $A = 0.028$ [82], with $A = E_v(Z) - E_v(Z+1)$].

The KS-SCE functional requires no special treatment for anions as it is able to bind them, though as usual its energy is far too low (see Fig. 8), resulting in severe overbinding [43]. The KS-SCE HOMO, however is often a good approximation to the affinity [34,43].

Variable N with $Z = 1$. We can see how close KS-NLR comes to binding two electrons by considering a hydrogen atom with a fractional number of electrons N. The exact energy as a function of N should be piecewise linear with kinks at integer N [99], and the HOMO energy (which is the derivative of the energy with respect to N) should be a series of steps jumping at integer N. For hydrogen, the exact behavior of the energy and the HOMO eigenvalue is plotted in Fig. 8, alongside KS-NLR, KS-LDA, and KS-SCE functionals. When spin-restricted, KS-LDA makes a fractional spin error for the neutral hydrogen atom ($N = 1$, $N_\uparrow = N_\downarrow = 1/2$) [100], which has consequences for dissociating H_2—we discuss this more for the 1D case later. On the other hand, KS-NLR and KS-SCE are exact for $N \leqslant 1$, but err substantially for $N > 1$. Nevertheless, there is a nonanalyticity in the energy (and thus in the HOMO) energies at $N = 1$ for KS-NLR and KS-SCE, unlike in KS-LDA, which is the sign that some of the right physics is being captured. Within time-dependent DFT, this behavior is crucial: nonanalytic behavior at the integers is
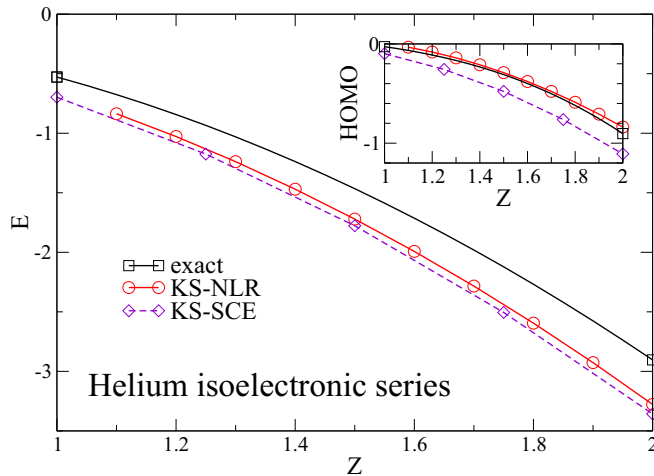
FIG. 9. (Color online) Self-consistent energies and HOMO eigenvalues of the KS-NLR and KS-SCE functionals for the 3D helium isoelectronic series ($N = 2$, Z variable), compared with the exact behavior (cubic spline interpolation of $Z = 1, 2, 4, 10$ values from Ref. [82]), KS-SCE data from Ref. [43].

TABLE III. Self-consistent atoms and ions within the KS-NLR method in three dimensions. Exact ionization energies are experimental values from Ref. [89].

Atom	$E^{\text{KS-NLR}}$	$I^{\text{KS-NLR}}$	$-\epsilon^{\text{KS-NLR}}_{\text{HOMO}}$	Accurate I
He	-3.278	1.278	0.84	0.904
Li	-8.170	0.279	0.16	0.198
Be	-15.76	0.45	0.29	0.343
Ne	-134.9	1.2	0.78	0.792

the key to to describe important phenomena as, e.g., charge transfer [101]. The strong correlation functionals KS-NLR and KS-SCE bind for larger values of N than KS-LDA, though KS-NLR stops short of binding for $N = 2$, as we have already noticed. But as can be seen, KS-NLR energetically looks a lot like KS-SCE, though intriguingly drops below KS-SCE for certain values of N.

Critical Z with N = 2. To investigate further, we decrease the nuclear charge Z in fractional amounts from 2 to 1, moving from He to H$^-$ [43]. If there were ever such a thing as fractionally charged nuclei, there is a critical value of Z below which two electrons would not bind: $Z_c \approx 0.9110$ [102,103]. In KS-NLR, however, we have already seen that the critical Z value is above 1, since hydrogen does not bind two electrons. In Fig. 9 we plot our self-consistent results for fractional Z. Using our numerical approach, we could easily converge down to $Z = 1.1$, so we anticipate the critical Z in KS-NLR near or just below that. In KS-SCE, there is no difficulty in binding extra electrons, and Z_c is severely underestimated: $Z_c \approx 0.7307$ [43].

We remark here that, as usual, KS-NLR energies track quite well along with the KS-SCE energies, though there is a fairly large gap in the HOMO energies due to the KS-NLR potential being higher than the KS-SCE potential. Interestingly, this makes the KS-NLR HOMO eigenvalues fairly close to the exact HOMO eigenvalues, and suggests that electron ionization energies might be well described by the KS-NLR HOMO energies. We investigate this in other systems next.

Many-electron 3D atoms. In Table III we report total energies, ionization energies $I = E_v(N-1) - E_v(N)$, and HOMO eigenvalues for atoms self-consistently calculated using the KS-NLR method. In exact KS-DFT, ϵ_{HOMO} should be equal to minus the exact, many-body, ionization potential I [104]. As expected from Fig. 8, the KS-NLR method does not give good agreement between its own ionization energies (computed by taking energy differences) and $-\epsilon_{\text{HOMO}}$. Instead,

the KS-NLR HOMO energies are reasonably close to the true I for the atoms in Table I: -7%, -19%, -15%, and -2% errors for He, Li, Be, and Ne, respectively.

As the atomic number Z gets larger, we expect KS-NLR to become asymptotically correct for the ionization energy, since exchange and correlation energies show up at smaller orders of Z than kinetic, Hartree, and potential energies for large atoms [105]. The KS-NLR interaction XC energy scales like exchange, though with a larger (in magnitude) coefficient. To quantify this, for large Z atoms, exchange dominates over correlation, and is locally $\epsilon_X(r_S) \approx -0.458/r_S$ [106], about 1.6 times smaller than the uniform gas limit of KS-NLR (48). Nonuniform effects certainly play a role, but will not affect higher orders of Z.

We now turn our attention to various 1D systems.

B. Parabolic traps in one dimension

Of interest in strong correlation physics is the confinement of electrons in low-dimensional nanostructures such as quantum wires and quantum dots [18,35]. We will consider the parabolic trap of Ref. [18] as a model for the quantum wire, though with the soft-Coulomb interactions of Ref. [51]. The external potential is then given by $v(x) = kx^2/2$. In a weakly correlated trap ($k \gtrsim 10^{-1}$ for our interactions), the quantum kinetic-energy operator dominates the physics of the electrons. This regime yields Friedel-type oscillations of wavelength $2k_F$, where $k_F = \pi \bar{n}/2$ is the effective Fermi wave number, with $\bar{n}$ the effective average density in the middle of the trap [18]. But as the confinement in the parabolic trap weakens ($k \ll 10^{-1}$), the Coulomb repulsion operator drives the electron physics, and we observe a $2k_F \to 4k_F$ transition in the wavelength of the density oscillations. Peaks form in the density where charge localizes, and these peaks are the tell-tale signs of a Wigner-like regime. The challenge in this kind of systems is to capture this crossover without introducing magnetic order (i.e., without symmetry breaking), something that has been tried with GGA and self-interaction corrections without success [107,108].

The KS-SCE functional captures this $2k_F \to 4k_F$ crossover [18], and so does the KS-NLR functional, without any symmetry breaking. We can see this in Fig. 10, which plots the densities of $N = 4$ electrons in parabolic traps with varying confinement strengths. As k becomes small, the strongly correlated KS-SCE and KS-NLR methods naturally produce peaks in the right locations. Neither method develops the peaks as strongly or as quickly as the exact result, but the KS-NLR method has a slight edge for very low densities. Unfortunately, the KS-NLR functional predicts an unphysical
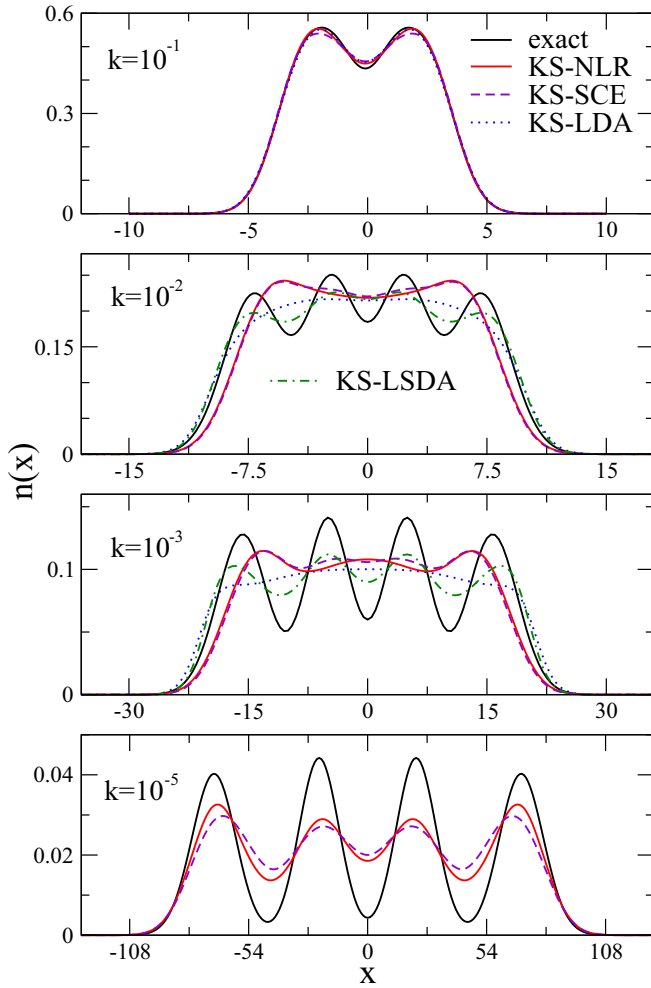
FIG. 10. (Color online) Densities of the $2k_F \to 4k_F$ transition for $N = 4$ soft-Coulomb interacting electrons in a parabolic external potential $v(x) = kx^2/2$. Exact density from DMRG [109].

transition region with three peaks near $k = 10^{-3}$, whereas the KS-SCE method correctly predicts only either two or four peaks. These density peaks are a result of barriers in the KS potentials [110], which we plot in Fig. 11 for $k = 10^{-5}$, and are well known to be of nonlocal nature [111].

For comparison in Fig. 10, we also have 1D LDA results using the correlation fit from Ref. [112] and exchange from
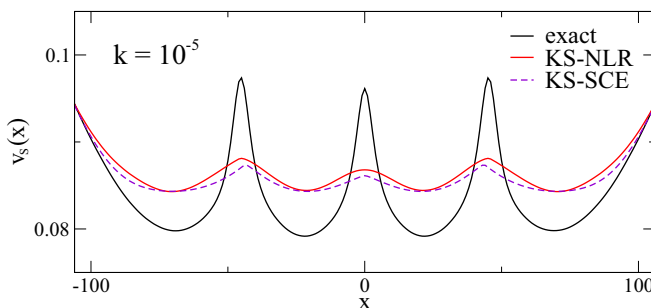

FIG. 11. (Color online) KS potentials for the $k = 10^{-5}$ system of Fig. 10.

Ref. [51]. While KS-LDA does well for weakly correlated systems (large k), things get worse for small k. Around $k = 0.01$, KS-LDA looks like the Thomas-Fermi solution, since the potential is very slowly varying. But as k gets even smaller, KS-LDA becomes very difficult to converge, as the density becomes very delocalized and a very large grid in needed [18]. By breaking spin symmetry [51], the local *spin*-density approximation (LSDA) method can achieve peaks [113]. However, these systems have no magnetic order, so density functionals should capture the physics without breaking symmetry. This is required on a more fundamental level for transition-metal oxides above the Néel temperature, where magnetic order is destroyed but strong charge localization (the insulating phase) is still present [114]. Notice that we could not converge either KS-LDA or KS-LSDA for very small k, i.e., $\leqslant 10^{-5}$. To date, only strongly correlated functionals like KS-SCE and KS-NLR correctly localize charge—without introducing magnetic order—in regions where the external potential offers no hints.

C. Simple 1D molecules

Here we investigate the binding energy curves of various 1D molecules, where we consider the total energies of the system for soft-Coulomb interacting systems. Thus we add the electronic energy and the interaction energy between nuclei:

$$E_0(R) \equiv E_v + \frac{Z_1 Z_2}{\sqrt{R^2 + 1}}, \qquad (55)$$

where $v(x) = -Z_1/\sqrt{x^2 + 1} - Z_2/\sqrt{(x - R)^2 + 1}$. This soft 1D universe is a laboratory to test functionals and ideas about correlation [51], where we have easy access to exact answers using the density-matrix renormalization group [109]. We will consider neutral systems with $N = Z_1 + Z_2$.

1D hydrogen molecule. We consider the most infamous example of bond breaking in KS-DFT: H_2. Standard KS-DFT methods fail to dissociate H_2 correctly because of *fractional spin error*: the energy of a single hydrogen atom with one spin-up (or one spin-down) electron is different than with half an up-spin and half a down-spin electron [100]. At dissociation, H_2 comprises two such spin-unpolarized atoms, whereas functionals typically give accurate values for a single H atom only when spin polarized. This difficulty occurs for all molecules which dissociate into open-shell fragments.

In Fig. 12 we plot the binding energy curve of H_2 for various functionals. At dissociation, KS-LDA errs due to its fractional spin error, whereas both strongly correlated methods KS-SCE and KS-NLR dissociate H_2 correctly, i.e., $E_0(R) \to 2E_H$ as $R \to \infty$. As in the parabolic 1D traps, breaking spin symmetry allows KS-LSDA to dissociate correctly [51,115] (not shown in Fig. 12, but see Refs. [34,51]), but with all the caveats mentioned for breaking spin symmetry in the parabolic traps. However, both strong correlation functionals bind the H_2 molecule much too strongly, and the well extends out to too large of R. Despite these gross chemical inaccuracies, the equilibrium bond length is overestimated by only 1% in KS-NLR and 3% in KS-SCE, whereas KS-LDA makes a 2% error [51].

We emphasize here that both KS-SCE and KS-NLR do not need to break spin symmetry to dissociate H_2 correctly.
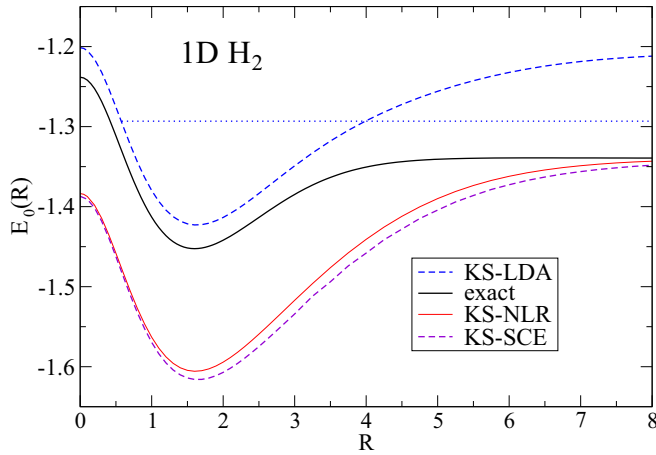
FIG. 12. (Color online) The total molecular energy of 1D H_2 with soft-Coulomb interactions between all particles. Exact and KS-LDA data from Ref. [51]. The horizontal dotted line is twice the energy of a KS-LSDA hydrogen atom.

FIG. 14. (Color online) The total molecular energy of 1D LiH with soft-Coulomb interactions between all particles. Horizontal lines indicate the sum of energies of an isolated Li atom and an isolated H atom within each method.

In fact, there is no spin dependence in either the NLR or SCE functional, so neither functional can lower the energy by breaking spin symmetry. Instead, breaking spin symmetry *raises* the kinetic energy of the KS wave function, and there is no corresponding decrease in the interaction energy (since it is spin independent). Thus a spin-unrestricted calculation within either KS-NLR or KS-SCE yields the same result as a spin-restricted calculation. See also Ref. [35] for a similar discussion with KS-SCE applied to parabolic traps.

1D helium dimer. We now consider a molecule which dissociates into closed-shell fragments, He_2. Here the issues of fractional spin disappear, since the fragments are closed shell. Dissociating He_2 yields two spin-unpolarized helium atoms, and standard KS-DFT approximations do well for spin-unpolarized helium atoms. See Fig. 13 for plots of the 1D He_2 binding energy. KS-LDA dissociates correctly (to the value of $2E_{He}^{KS-LDA}$), as do the strongly correlated methods.

In three dimensions, there is a very weak van der Waals bond for the helium dimer; but soft-Coulomb 1D He_2 has no bound state. Here KS-SCE incorrectly predicts a weakly bound state.

1D lithium hydride. Here is another example of dissociating into open-shell fragments: lithium ($Z_1 = 3$) hydride ($Z_2 = 1$). See Fig. 14 for a plot of the binding-energy curve. Much of the discussion on H_2 carries over for LiH. KS-LDA makes an error in the dissociation limit due to fractional-spin error, whereas KS-SCE and KS-NLR do not. Both KS-NLR and KS-SCE methods overbind. Here we found it challenging to converge the KS-SCE method for large R values, and there is some numerical noise in the KS-SCE data due to the integration methods used. As can be seen in Fig. 14, KS-NLR is going very slowly to its dissociation limit. This is due to the long-ranged behavior of the NLR interaction XC energy per particle, $w_{XC}^{NLR}(x)$, as seen in, e.g., Fig. 3 (and see nearby discussion).

V. FUTURE WORK AND CONCLUSIONS

This work lays the mathematical foundation for the application of an approximate functional (called NLR) for the strong-interaction limit of DFT, using the nonlocal Wigner-Seitz radius $R(\mathbf{r})$. This functional is capable of dissociating single bonds and localizing charge density, key signatures of strong correlation physics, and it is computationally much more accessible than the exact strong-correlation limit of DFT, SCE. The energy as a function of the number of electrons N displays nonanalyticities at integer N even for open-shell systems in a spin-restricted formalism, although we do not fully capture the correct energy versus N piecewise linear behavior. In its present form, however, the functional may not bind negative ions, and its potential does not have the right asymptotic behavior. We envision many avenues of future research, which build upon the ideas presented in this work and seek to correct the deficiencies of the NLR functional.

The main challenge is to build corrections to our functional that add the accuracy of standard DFT for weakly and moderately correlated systems without destroying the ability
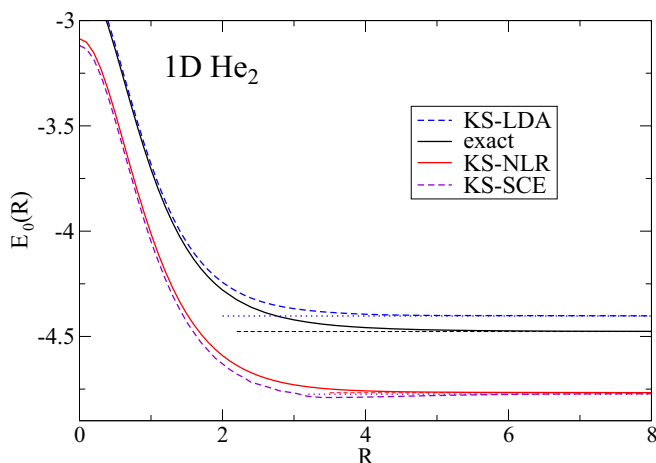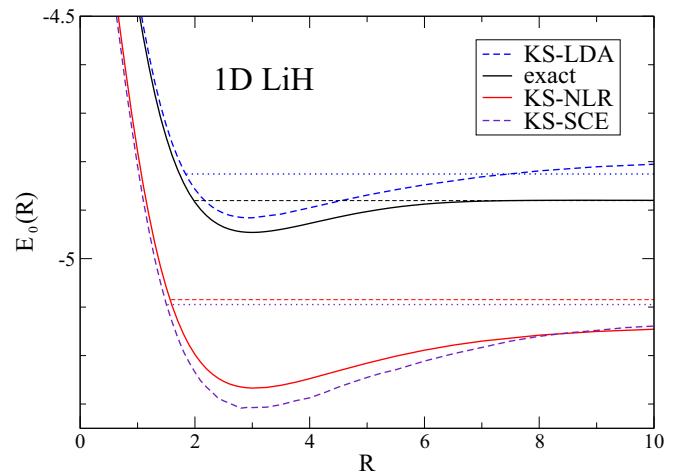

FIG. 13. (Color online) (Lack of) binding for the 1D soft-Coulomb helium dimer. KS-SCE predicts a weakly bound state. Horizontal lines indicate twice the energy of a single isolated helium atom within each method.

of NLR to capture strong-correlation features, and, possibly, to improve them. One can produce corrections to make the nonlocal method correct for the uniform gas [18], as well as one-electron systems, by using the nonlocal Wigner-Seitz radius $R(\mathbf{r})$ in place of (or somehow combined with) the local $r_S(\mathbf{r})$ in the LDA XC energy density. Since $R(\mathbf{r}) \rightarrow 0$ for one-electron systems, the XC energy density will also go to zero. Despite the simplicity of this approach, there are many free parameters which affect the transition from one electron to many. This nonlocal LDA is the subject of current work. Suitable corrections may also fix the asymptotic behavior of the NLR XC potential.

Using the energy density of the NLR functional to create a local interpolation along the adiabatic connection, using the exact (or an approximate) exchange energy density for the weakly correlated limit seems also a very promising route of action.

The introduction of spin densities usually helps in obtaining better energies and to treat open-shell systems. There are many ways to generalize the nonlocal machinery to spin-polarized systems. Here we suggest just one way: continue to define the nonlocal radius $R(\mathbf{r})$ using the total density, but then define the polarization via an average of the local polarization within the nonlocal Wigner-Seitz sphere $\Omega(\mathbf{r})$:

$$\zeta(\mathbf{r}) = \int_{\Omega(\mathbf{r})} d^3r' \, (n_\uparrow(\mathbf{r}') - n_\downarrow(\mathbf{r}')). \tag{56}$$

This will equal 1 if $n_\uparrow(\mathbf{r}) = n(\mathbf{r})$ in the Wigner-Seitz sphere $\Omega(\mathbf{r})$, will equal -1 if $n_\downarrow(\mathbf{r}) = n(\mathbf{r})$, and will otherwise land somewhere in between. For an unpolarized electron density, $n_\uparrow(\mathbf{r}) = n_\downarrow(\mathbf{r})$ so $\zeta(\mathbf{r}) = 0$. Using the nonlocal $\zeta(\mathbf{r})$ in place of the local version might well complement the nonlocal LDA strategy outlined above.

For a completely different application, one can use $R(\mathbf{r})$ to develop a nonlocal orbital-free kinetic-energy functional [as in the original paper [80] which inspired the definition of $R(\mathbf{r})$], by writing the Thomas-Fermi kinetic energy using $R(\mathbf{r})$ and/or combining with the von Weizsäcker kinetic energy. Again there are many free parameters even after constraints to yield the correct limits for the uniform gas and one-electron systems.

APPENDIX A: CALCULATING $R(\mathbf{r})$

In general, to calculate $R(\mathbf{r})$ we need to be able to integrate the density in a sphere concentric with the point $\mathbf{r}$ with an arbitrary radius R:

$$N_e(\mathbf{r}, R) \equiv \int d^3r' \, n(\mathbf{r}') \, \theta(R - |\mathbf{r} - \mathbf{r}'|). \tag{A1}$$

If we can fit the density to a sum of Gaussian or Slater-type exponentials, this integral becomes an analytical function of R. An alternative, basis-independent approach is to use information from the Hartree potential. We can then obtain $R(\mathbf{r})$ by finding the root $N_e(\mathbf{r}, R(\mathbf{r})) = 1$. Since $N_e(\mathbf{r}, R)$ is monotonically increasing in R, we easily obtain the root by increasing the radius from zero or by using Newton's shooting method.

Evaluating $N_e(\mathbf{r}, R)$ for Gaussian-type densities. Imagine that your density is well described by a single Gaussian centered at $\hat{z}b$ with decay constant α, i.e., $n(\mathbf{r}) = e^{-\alpha|\mathbf{r}-\hat{z}b|^2}$. (Later we will sum over many such terms.) We now integrate the density in a sphere of radius R concentric with the origin. The number of electrons in that sphere is

$$N_b^{G,\alpha}(R) \equiv \int d^3r \, e^{-\alpha|\mathbf{r}-b\hat{z}|^2} \theta(R - |\mathbf{r}|). \tag{A2}$$

This may be evaluated quite easily:

$$N_b^{G,\alpha}(R) = -\pi \frac{1 - e^{-4\alpha b R}}{2\alpha^2 b} e^{-G_-^2}$$

$$+ \frac{1}{2} \left(\frac{\pi}{\alpha}\right)^{3/2} (\mathrm{erf}\, G_+ + \mathrm{erf}\, G_-), \tag{A3}$$

where $G_\pm \equiv \sqrt{\alpha}(R \pm b)$. Alternatively, we can first calculate the density of electrons integrated over the surface of a sphere of radius R, where the center of the sphere is displaced a distance b from the center of the Gaussian of decay α:

$$S_b^{G,\alpha}(R) \equiv R^2 \int_{4\pi} d\Omega_{\hat{u}} \, e^{-\alpha|R\hat{u}-b\hat{z}|^2}. \tag{A4}$$

This analytically integrates to

$$S_b^{G,\alpha}(R) = \frac{\pi R}{\alpha b} e^{-G_-^2} (1 - e^{-4\alpha b R}). \tag{A5}$$

Then we can calculate $N_b^{G,\alpha}(R)$ by integrating $S_b^{G,\alpha}(R')$ from $R' = 0$ to R.

We now use this information in order to calculate $R(\mathbf{r})$ when the density is a sum of such Gaussians:

$$n(\mathbf{r}) = \sum_j g_j e^{-\alpha_j|\mathbf{r}-\mathbf{R}_j|^2}. \tag{A6}$$

For this density, we now find the number of electrons in a sphere of radius R, centered at $\mathbf{r}$. To do this, we use Eq. (A2) and shift the origin for each term in the sum (A6):

$$N_e(\mathbf{r}, R) = \sum_j g_j N_{|\mathbf{r}-\mathbf{R}_j|}^{G,\alpha_j}(R). \tag{A7}$$

And we find $R(\mathbf{r})$ by finding the root $N_e(\mathbf{r}, R(\mathbf{r})) = 1$ as discussed earlier.

Evaluating $N_e(\mathbf{r}, R)$ for Slater-type densities. Similarly, we evaluate the number of electrons in a sphere of radius R at a distance b away from a Slater-type function with decay

constant α:

$$N_b^{S,\alpha}(R) \equiv \int d^3r \, e^{-\alpha|\mathbf{r}-b\hat{z}|} \theta(R - |\mathbf{r}|). \qquad (A8)$$

And by evaluation,

$$N_b^{S,\alpha}(R) = \begin{cases} N_<^S, & R < b, \\ N_>^S, & \text{otherwise,} \end{cases} \qquad (A9)$$

where

$$N_<^S = \frac{4\pi e^{-\alpha b}}{\alpha^4 b}(\alpha R \,(3 + \alpha b)\cosh\alpha R \\ - (3 + \alpha b + \alpha^2 R^2)\sinh\alpha R), \qquad (A10)$$

and

$$N_>^S = \frac{8\pi}{\alpha^3} + \frac{4\pi e^{-\alpha R}}{\alpha^4 b}(\alpha b(1 + \alpha R)\cosh\alpha b \\ - (3 + 3\alpha R + \alpha^2 R^2)\sinh\alpha b). \qquad (A11)$$

If we expand the density in a sum of Slater-type functions,

$$n(\mathbf{r}) = \sum_j s_j e^{-\alpha_j|\mathbf{r}-\mathbf{R}_j|}, \qquad (A12)$$

then $N_e(\mathbf{r}, R)$ is a simple sum:

$$N_e(\mathbf{r}, R) = \sum_j s_j \, N_{|\mathbf{r}-\mathbf{R}_j|}^{S,\alpha_j}(R). \qquad (A13)$$

Evaluating $N_e(\mathbf{r}, R)$ using Gauss' law. Gauss' law allows us to determine the charge Q contained in a volume Ω by integrating the electric field $\mathbf{E}(\mathbf{r})$ permeating the surface $\partial\Omega$ of the volume. In atomic units:

$$Q = \frac{1}{4\pi} \oint_{\partial\Omega} d\mathbf{A}(\mathbf{r}) \cdot \mathbf{E}(\mathbf{r}). \qquad (A14)$$

For electrons, the field is the gradient of the Hartree potential: $\mathbf{E}(\mathbf{r}) = \nabla v_{\text{H}}[n](\mathbf{r})$. Taking care with signs, the number of electrons in a sphere of radius R, centered at $\mathbf{r}$ is

$$N_e(\mathbf{r}, R) = -\frac{R^2}{4\pi} \int_{4\pi} d\Omega_{\hat{u}} \frac{\partial v_{\text{H}}[n](\mathbf{r} + R\hat{u})}{\partial R}. \qquad (A15)$$

We have not checked the efficiency of this approach, but we include it here in case it proves useful.

APPENDIX B: EVALUATING FUNCTIONAL DERIVATIVES

Here we derive $v_{\text{XC}}^{\text{NLR}}[n](\mathbf{r}) = \delta W_{\text{XC}}^{\text{NLR}}[n]/\delta n(\mathbf{r})$ by first determining how the NL radius $R(\mathbf{r})$ changes when the density changes by a small amount $\delta n(\mathbf{r})$. One may implicitly differentiate the definition of $R(\mathbf{r})$ in Eq. (32) and obtain

$$\delta R(\mathbf{r}) = \frac{-1}{S(\mathbf{r})} \int_{\Omega(\mathbf{r})} d^3r' \, \delta n(\mathbf{r}'), \qquad (B1)$$

where $\Omega(\mathbf{r})$ is the sphere defined by the original Wigner-Seitz radius $R(\mathbf{r})$, and $S(\mathbf{r})$ is the *nonlocal radial density* (with units of length^{-1}), defined by integrating the density over the surface $\partial\Omega(\mathbf{r})$ of the nonlocal Wigner-Seitz sphere, which can be performed in many different ways:

$$S(\mathbf{r}) \equiv \int_{\partial\Omega(\mathbf{r})} d^2r' \, n(\mathbf{r}') \qquad (B2)$$

$$= R^2(\mathbf{r}) \int_{4\pi} d\Omega_{\hat{u}} \, n(\mathbf{r} + R(\mathbf{r})\hat{u}) \qquad (B3)$$

$$= \int d^3r' \, n(\mathbf{r}') \, \delta(R(\mathbf{r}) - |\mathbf{r} - \mathbf{r}'|) \qquad (B4)$$

$$= \left.\frac{\partial N_e(\mathbf{r}, R)}{\partial R}\right|_{R=R(\mathbf{r})}. \qquad (B5)$$

To use the chain rule in functional derivatives, we rewrite Eq. (B1) as

$$\frac{\delta R(\mathbf{r})}{\delta n(\mathbf{r}')} = \frac{-1}{S(\mathbf{r})}\theta(R(\mathbf{r}) - |\mathbf{r} - \mathbf{r}'|). \qquad (B6)$$

Now to determine the NLR XC potential. The density appears in many different places inside $W_{\text{XC}}^{\text{NLR}}[n]$, so we get a few different terms as the density varies:

$$v_{\text{XC}}^{\text{NLR}}[n](\mathbf{r})$$
$$= -\frac{1}{2}\frac{\delta}{\delta n(\mathbf{r})} \int d^3r' \int d^3r'' \frac{n(\mathbf{r}')\,n(\mathbf{r}'')}{|\mathbf{r}'-\mathbf{r}''|}$$
$$\times \theta(R(\mathbf{r}') - |\mathbf{r}'-\mathbf{r}''|)$$
$$= -\frac{1}{2} \int d^3r'' \frac{n(\mathbf{r}'')}{|\mathbf{r}-\mathbf{r}''|}\theta(R(\mathbf{r}) - |\mathbf{r}-\mathbf{r}''|)$$
$$- \frac{1}{2} \int d^3r' \frac{n(\mathbf{r}')}{|\mathbf{r}'-\mathbf{r}|}\theta(R(\mathbf{r}') - |\mathbf{r}'-\mathbf{r}|)$$
$$- \frac{1}{2} \int d^3r' \frac{\delta R(\mathbf{r}')}{\delta n(\mathbf{r})} \int d^3r'' \frac{n(\mathbf{r}')\,n(\mathbf{r}'')}{|\mathbf{r}'-\mathbf{r}''|}$$
$$\times \delta(R(\mathbf{r}') - |\mathbf{r}'-\mathbf{r}''|). \qquad (B7)$$

The first two terms can be combined using $g_{\text{XC}}^{\text{NLR}}(\mathbf{r},\mathbf{r}')$, and in the third term we use our new relation from Eq. (B6) as well as the δ function to collapse $|\mathbf{r}'-\mathbf{r}''| \to R(\mathbf{r}')$:

$$v_{\text{XC}}^{\text{NLR}}[n](\mathbf{r})$$
$$= \int d^3r' \frac{n(\mathbf{r}')}{|\mathbf{r}-\mathbf{r}'|} g_{\text{XC}}^{\text{NLR}}(\mathbf{r},\mathbf{r}')$$
$$- \frac{1}{2} \int d^3r' \left[\left(\frac{-1}{S(\mathbf{r}')}\theta(R(\mathbf{r}') - |\mathbf{r}-\mathbf{r}'|) \right) \frac{n(\mathbf{r}')}{R(\mathbf{r}')} \right]$$
$$\times \int d^3r'' n(\mathbf{r}'')\,\delta(R(\mathbf{r}') - |\mathbf{r}'-\mathbf{r}''|)$$
$$= \int d^3r' \frac{n(\mathbf{r}')}{|\mathbf{r}-\mathbf{r}'|} g_{\text{XC}}^{\text{NLR}}(\mathbf{r},\mathbf{r}')$$
$$+ \frac{1}{2} \int d^3r' \left[\frac{n(\mathbf{r}')}{S(\mathbf{r}')\,R(\mathbf{r}')}\theta(R(\mathbf{r}') - |\mathbf{r}-\mathbf{r}'|) \right] S(\mathbf{r}'), \qquad (B8)$$

where to get to the last line we used Eq. (B4). Thus the $S(\mathbf{r}')$ cancels in this second integral, leaving us with Eq. (39).

[1] A. J. Cohen, P. Mori-Sánchez, and W. Yang, Chem. Rev. **112**, 289 (2012).

[2] A. D. Becke, J. Chem. Phys. **140**, 18A301 (2014).

[3] S. R. White, Phys. Rev. Lett. **69**, 2863 (1992).

[4] S. R. White, Phys. Rev. B **48**, 10345 (1993).

[5] U. Schollwöck, Rev. Mod. Phys. **77**, 259 (2005).

[6] S. R. White and R. L. Martin, J. Chem. Phys. **110**, 4127 (1999).

[7] G. K.-L. Chan, J. J. Dorando, D. Ghosh, J. Hachmann, E. Neuscamman, H. Wang, and T. Yanai, Prog. Theor. Chem. Phys. **18**, 49 (2008).

[8] G. K.-L. Chan and S. Sharma, Annu. Rev. Phys. Chem. **62**, 465 (2011).

[9] W. Kohn and L. J. Sham, Phys. Rev. **140**, A1133 (1965).

[10] J. P. Perdew, K. Burke, and M. Ernzerhof, Phys. Rev. Lett. **77**, 3865 (1996); **78**, 1396(E) (1997).

[11] A. D. Becke, Phys. Rev. A **38**, 3098 (1988).

[12] A. D. Becke, J. Chem. Phys. **98**, 5648 (1993).

[13] J. Heyd, G. E. Scuseria, and M. Ernzerhof, J. Chem. Phys. **118**, 8207 (2003); **124**, 219906(E) (2006).

[14] M. Seidl, Phys. Rev. A **60**, 4387 (1999).

[15] M. Seidl, P. Gori-Giorgi, and A. Savin, Phys. Rev. A **75**, 042511 (2007).

[16] P. Gori-Giorgi, G. Vignale, and M. Seidl, J. Chem. Theory Comput. **5**, 743 (2009).

[17] F. Malet and P. Gori-Giorgi, Phys. Rev. Lett. **109**, 246402 (2012).

[18] F. Malet, A. Mirtschink, J. C. Cremon, S. M. Reimann, and P. Gori-Giorgi, Phys. Rev. B **87**, 115146 (2013).

[19] J. P. Perdew and K. Schmidt, in *Density Functional Theory and Its Application to Materials*, edited by V. Van Doren *et al.* (AIP, Melville, NY, 2001), pp. 1–20.

[20] J. P. Perdew, A. Ruzsinszky, J. Tao, V. N. Staroverov, G. E. Scuseria, and G. I. Csonka, J. Chem. Phys. **123**, 062201 (2005).

[21] J. P. Perdew and Y. Wang, Phys. Rev. B **45**, 13244 (1992).

[22] C. Lee, W. Yang, and R. G. Parr, Phys. Rev. B **37**, 785 (1988).

[23] J. Tao, J. P. Perdew, V. N. Staroverov, and G. E. Scuseria, Phys. Rev. Lett. **91**, 146401 (2003).

[24] K. Burke, M. Ernzerhof, and J. P. Perdew, Chem. Phys. Lett. **265**, 115 (1997).

[25] J. P. Perdew and A. Zunger, Phys. Rev. B **23**, 5048 (1981).

[26] M. R. Pederson, A. Ruzsinszky, and J. P. Perdew, J. Chem. Phys. **140**, 121103 (2014).

[27] S. Grimme, J. Chem. Phys. **124**, 034108 (2006).

[28] J. Paier, X. Ren, P. Rinke, G. E. Scuseria, A. Grneis, G. Kresse, and M. Scheffler, New J. Phys. **14**, 043002 (2012).

[29] J. A. Alonso and L. A. Girifalco, Solid State Commun. **24**, 135 (1977).

[30] J. A. Alonso and L. A. Girifalco, Phys. Rev. B **17**, 3735 (1978).

[31] M. Jonson O. Gunnarsson and B. I. Lundqvist, Solid State Commun. **24**, 765 (1977).

[32] O. Gunnarsson, M. Jonson, and B. I. Lundqvist, Phys. Rev. B **20**, 3136 (1979).

[33] R. M. Dreizler and E. K. U. Gross, *Density Functional Theory: An Approach to the Quantum Many-Body Problem* (Springer-Verlag, Berlin, 1990).

[34] F. Malet, A. Mirtschink, K. J. H. Giesbertz, L. O. Wagner, and P. Gori-Giorgi, Phys. Chem. Chem. Phys. **16**, 14551 (2014).

[35] C. B. Mendl, F. Malet, and P. Gori-Giorgi, Phys. Rev. B **89**, 125106 (2014).

[36] G. Buttazzo, L. De Pascale, and P. Gori-Giorgi, Phys. Rev. A **85**, 062502 (2012).

[37] B. Pass, J. Funct. Anal. **264**, 947 (2013).

[38] C. Cotar, G. Friesecke, and C. Klüppelberg, Commun. Pure Appl. Math. **66**, 548 (2013).

[39] C. B. Mendl and Lin L., Phys. Rev. B **87**, 125106 (2013).

[40] H. Chen, G. Friesecke, and C. B. Mendl, arXiv:1405.7026.

[41] G. Friesecke, C. B. Mendl, B. Pass, C. Cotar, and C. Klüppelberg, J. Chem. Phys. **139**, 164109 (2013).

[42] C. Villani, *Topics in Optimal Transportation*, Graduate Studies in Mathematics No. 58 (American Mathematical Society, Providence, 2003).

[43] A. Mirtschink, C. J. Umrigar, J. D. Morgan, and P. Gori-Giorgi, J. Chem. Phys. **140**, 18 (2014).

[44] M. Seidl, J. P. Perdew, and S. Kurth, Phys. Rev. A **62**, 012502 (2000); **72**, 029904(E) (2005).

[45] M. Seidl, J. P. Perdew, and S. Kurth, Phys. Rev. Lett. **84**, 5070 (2000).

[46] K. Burke, in *Electronic Density Functional Theory: Recent Progress and New Directions*, edited by J. F. Dobson, G. Vignale, and M. P. Das (Plenum, New York, 1997), pp. 19–29.

[47] P. Gori-Giorgi, J. G. Angyan, and A. Savin, Can. J. Chem. **87**, 1444 (2009).

[48] L. Onsager, J. Phys. Chem. **43**, 189 (1939).

[49] A. Mirtschink, M. Seidl, and P. Gori-Giorgi, J. Chem. Theory Comput. **8**, 3097 (2012).

[50] S. Vuckovic, L. O. Wagner, A. Mirtschink, and P. Gori-Giorgi, (unpublished).

[51] L. O. Wagner, E. M. Stoudenmire, K. Burke, and S. R. White, Phys. Chem. Chem. Phys. **14**, 8581 (2012).

[52] P. Hohenberg and W. Kohn, Phys. Rev. **136**, B864 (1964).

[53] M. Levy, Proc. Natl. Acad. Sci. USA **76**, 6062 (1979).

[54] E. H. Lieb, Int. J. Quantum Chem. **24**, 243 (1983).

[55] S. M. Valone, J. Chem. Phys. **73**, 4653 (1980).

[56] M. Levy, Phys. Rev. A **26**, 1200 (1982).

[57] C. A. Ullrich and W. Kohn, Phys. Rev. Lett. **87**, 093001 (2001).

[58] R. van Leeuwen, Adv. Quant. Chem. **43**, 25 (2003).

[59] L. O. Wagner, E. M. Stoudenmire, K. Burke, and S. R. White, Phys. Rev. Lett. **111**, 093003 (2013).

[60] A. Görling, Phys. Rev. A **46**, 3753 (1992).

[61] Y. Wang and R. G. Parr, Phys. Rev. A **47**, R1591 (1993).

[62] K. L. Laidig, Chem. Phys. Lett. **225**, 285 (1994).

[63] Q. Zhao, R. C. Morrison, and R. G. Parr, Phys. Rev. A **50**, 2138 (1994).

[64] R. Leeuwen, O. V. Gritsenko, and E. J. Baerends, in *Density Functional Theory I*, Topics in Current Chemistry Vol. 180, edited by R. F. Nalewajski (Springer, Berlin, Heidelberg, 1996), pp. 107–167.

[65] P. R. T. Schipper, O. V. Gritsenko, and E. J. Baerends, Theor. Chem. Acc. **98**, 16 (1997).

[66] K. Peirs, D. Van Neck, and M. Waroquier, Phys. Rev. A **67**, 012505 (2003).

[67] L. O. Wagner, T. E. Baker, E. M. Stoudenmire, K. Burke, and S. R. White, Phys. Rev. B **90**, 045109 (2014).

[68] P. W. Ayers and M. Levy, J. Chem. Sci. **117**, 507 (2005).

[69] D. C. Langreth and J. P. Perdew, Solid State Commun. **17**, 1425 (1975).

[70] O. Gunnarsson and B. I. Lundqvist, Phys. Rev. B **13**, 4274 (1976).

[71] P. Gori-Giorgi and J. P. Perdew, Phys. Rev. B **66**, 165118 (2002).

[72] K. Burke, J. P. Perdew, and D. C. Langreth, Phys. Rev. Lett. **73**, 1283 (1994).

[73] K. Burke and J. P. Perdew, Int. J. Quantum Chem. **56**, 199 (1995).

[74] K. Burke, J. P. Perdew, and M. Ernzerhof, J. Chem. Phys. **109**, 3760 (1998).

[75] R. O. Jones and O. Gunnarsson, Rev. Mod. Phys. **61**, 689 (1989).

[76] J. P. Perdew, in *Electronic Structure of Solids '91*, edited by P. Ziesche and H. Eschrig (Akademie Verlag, Berlin, 1991), pp. 11–20.

[77] P. Gori-Giorgi, M. Seidl, and G. Vignale, Phys. Rev. Lett. **103**, 166402 (2009).

[78] P. Gori-Giorgi and M. Seidl, Phys. Chem. Chem. Phys. **12**, 14405 (2010).

[79] M. Colombo, L. De Pascale, and S. Di Marino, Can. J. Math., doi:10.4153/CJM-2014-011-x.

[80] C. Herring, Phys. Rev. A **34**, 2614 (1986).

[81] G. F. Giuliani and G. Vignale, *Quantum Theory of the Electron Liquid* (Cambridge University Press, New York, 2005).

[82] C. J. Umrigar and X. Gonze, Phys. Rev. A **50**, 3827 (1994).

[83] C. Filippi, X. Gonze, and C. J. Umrigar, *Recent Developments and Applications of Density Functional Theory*, edited by J. M. Seminario (Elsevier, Amsterdam, 1996), pp. 295–326.

[84] A. I. Al-Sharif, R. Resta, and C. J. Umrigar, Phys. Rev. A **57**, 2466 (1998).

[85] M. W. Schmidt, K. K. Baldridge, J. A. Boatz, S. T. Elbert, M. S. Gordon, J. J. Jensen, S. Koseki, N. Matsunaga, K. A. Nguyen, S. Su, T. L. Windus, M. Dupuis, and J. A. Montgomery, J. Comput. Chem. **14**, 1347 (1993).

[86] F. Weigend, A. Kohn, and C. Hattig, J. Chem. Phys. **116**, 3175 (2002).

[87] F. G. Cruz, K.-C. Lam, and K. Burke, J. Phys. Chem. A **102**, 4911 (1998).

[88] A. Savin, H. Stoll, and H. Preuss, Theor. Chim. Acta **70**, 407 (1986).

[89] *NIST Computational Chemistry Comparison and Benchmark Database*, edited by R. D. Johnson III, release 15b ed., NIST Standard Reference Database Number 101, 2011, http://cccbdb.nist.gov/.

[90] K. Burke, F. G. Cruz, and K.-C. Lam, J. Chem. Phys. **109**, 8161 (1998).

[91] A. V. Arbuznikov and M. Kaupp, J. Chem. Phys. **128**, 214107 (2008).

[92] M. Ernzerhof, Chem. Phys. Lett. **263**, 499 (1996).

[93] W. Kolos and L. Wolniewicz, J. Chem. Phys. **49**, 404 (1968).

[94] D. R. Hartree, Math. Proc. Cambridge Philos. Soc. **24**, 426 (1928).

[95] R. Cuevas-Saavedra, D. Chakraborty, S. Rabi, C. Cárdenas, and P. W. Ayers, J. Chem. Theory Comput. **8**, 4081 (2012).

[96] E. Wigner, Phys. Rev. **46**, 1002 (1934).

[97] J. G. Vilhena, E. Räsänen, M. A. L. Marques, and S. Pittalis, J. Chem. Theory Comput. **10**, 1837 (2014).

[98] M.-C. Kim, E. Sim, and K. Burke, J. Chem. Phys. **134**, 171103 (2011).

[99] J. P. Perdew, R. G. Parr, M. Levy, and J. L. Balduz, Phys. Rev. Lett. **49**, 1691 (1982).

[100] A. J. Cohen, P. Mori-Sánchez, and W. Yang, Science **321**, 792 (2008).

[101] M. Hellgren and E. K. U. Gross, Phys. Rev. A **85**, 022514 (2012).

[102] J. D. Baker, D. E. Freund, R. Nyden Hill, and J. D. Morgan III, Phys. Rev. A **41**, 1247 (1990).

[103] C. S. Estienne, M. Busuttil, A. Moini, and G. W. F. Drake, Phys. Rev. Lett. **112**, 173001 (2014); **113**, 039902(E) (2014).

[104] M. Levy, J. P. Perdew, and V. Sahni, Phys. Rev. A **30**, 2745 (1984).

[105] D. Lee, L. A. Constantin, J. P. Perdew, and K. Burke, J. Chem. Phys. **130**, 034107 (2009).

[106] P. A. M. Dirac, Math. Proc. Cambridge Philos. Soc. **26**, 376 (1930).

[107] D. Vieira and K. Capelle, J. Chem. Theory Comput. **6**, 3319 (2010).

[108] D. Vieira, Phys. Rev. B **86**, 075132 (2012).

[109] E. M. Stoudenmire, L. O. Wagner, S. R. White, and K. Burke, Phys. Rev. Lett. **109**, 056402 (2012).

[110] J. P. Perdew, in *Density Functional Methods in Physics*, edited by R. M. Dreizler and J. da Providencia (Plenum, New York, 1985), pp. 265–308.

[111] N. Helbig, I. V. Tokatly, and A. Rubio, J. Chem. Phys. **131**, 224105 (2009).

[112] N. Helbig, J. I. Fuks, M. Casula, M. J. Verstraete, M. A. L. Marques, I. V. Tokatly, and A. Rubio, Phys. Rev. A **83**, 032503 (2011).

[113] S. H. Abedinpour, M. Polini, G. Xianlong, and M. P. Tosi, Phys. Rev. A **75**, 015602 (2007).

[114] V. I. Anisimov, J. Zaanen, and O. K. Andersen, Phys. Rev. B **44**, 943 (1991).

[115] C. A. Coulson and I. Fischer, Philoso. Mag. Ser. 7 **40**, 386 (1949).